Available online at www.sciencedirect.com
ScienceDirect
Geochimica et Cosmochimica Acta 75 (2011) 4929–4950
Geochimica et Cosmochimica Acta
www.elsevier.com/locate/gca

Speleothem calcite farmed *in situ*: Modern calibration of $\delta^{18}O$ and $\delta^{13}C$ paleoclimate proxies in a continuously-monitored natural cave system

Darrel M. Tremaine [a,*], Philip N. Froelich [b], Yang Wang [a]

[a] *Florida State University, Department of Earth Ocean and Atmospheric Science, National High Magnetic Field Laboratory, 1800 E. Paul Dirac Drive, Tallahassee, FL 32310-3706, United States*
[b] *Froelich Education Services, 3402 Cameron Chase Drive, Tallahassee, FL 32309-2898, United States*

Received 23 December 2010; accepted in revised form 2 June 2011; available online 16 June 2011

Abstract

Understanding the relationships between speleothem stable isotopes ($\delta^{13}C$ $\delta^{18}O$) and *in situ* cave forcing mechanisms is important to interpreting ancient stalagmite paleoclimate records. Cave studies have demonstrated that the $\delta^{18}O$ of inorganically precipitated (low temperature) speleothem calcite is systematically heavier than the $\delta^{18}O$ of laboratory-grown calcite for a given temperature. To understand this apparent offset, rainwater, cave drip water, groundwater, and modern naturally precipitated calcite (farmed *in situ*) were grown at multiple locations inside Hollow Ridge Cave in Marianna, Florida. High resolution micrometeorological, air chemistry time series and ventilation regimes were also monitored continuously at two locations inside the cave, supplemented with periodic bi-monthly air gas grab sample transects throughout the cave.

Cave air chemistry and isotope monitoring reveal density-driven airflow pathways through Hollow Ridge Cave at velocities of up to 1.2 m s^{-1} in winter and 0.4 m s^{-1} in summer. Hollow Ridge Cave displays a strong ventilation gradient in the front of the cave near the entrances, resulting in cave air that is a mixture of soil gas and atmospheric CO_2. A clear relationship is found between calcite $\delta^{13}C$ and cave air ventilation rates estimated by proxies pCO_2 and ^{222}Rn. Calcite $\delta^{13}C$ decreased linearly with distance from the front entrance to the interior of the cave during all seasons, with a maximum entrance-to-interior gradient of $\Delta\delta^{13}C_{CaCO3} = -7‰$. A whole-cave "Hendy test" at multiple contemporaneous farming sites reveals that ventilation induces a $+1.9 \pm 0.96‰$ $\delta^{13}C$ offset between calcite precipitated in a ventilation flow path and calcite precipitated on the edge or out of flow paths. This interpretation of the "Hendy test" has implications for interpreting $\delta^{13}C$ records in ancient speleothems. Calcite $\delta^{13}C_{CaCO3}$ may be a proxy not only for atmospheric CO_2 or overlying vegetation shifts but also for changes in cave ventilation due to dissolution fissures and ceiling collapse creating and plugging ventilation windows.

Farmed calcite $\delta^{18}O$ was found to exhibit a $+0.82 \pm 0.24‰$ offset from values predicted by both theoretical calculations and laboratory-grown inorganic calcite. Unlike $\delta^{13}C_{CaCO3}$, oxygen isotopes showed no ventilation effects, i.e. $\Delta\delta^{18}O_{CaCO3}$ appears to be a function of growth temperature only although we cannot rule out a small effect of (unmeasured) gradients in relative humidity (evaporation) accompanying ventilation. Our results support the findings of other cave investigators that water–calcite fractionation factors observed in speleothem calcite are higher that those measured in laboratory experiments. Cave and laboratory calcite precipitates may differ mainly in the complex effects of kinetic isotope fractionation. Combining our data with other recent speleothem studies, we find a new empirical relationship for cave-specific water–calcite oxygen isotope fractionation across a range of temperatures and cave environments:

$$1000 \ln \alpha = 16.1\left(10^3 T^{-1}\right) - 24.6$$

with a fractionation temperature dependence of $\Delta\delta^{18}O/\Delta T = -0.177‰/°C$, lower than the currently accepted $-0.206‰/°C$.
© 2011 Elsevier Ltd. All rights reserved.

* Corresponding author.
E-mail address: tremaine@magnet.fsu.edu (D.M. Tremaine).

0016-7037/$ - see front matter © 2011 Elsevier Ltd. All rights reserved.
doi:10.1016/j.gca.2011.06.005

1. INTRODUCTION

Calcite ($CaCO_3$) cave formations, or speleothems, incorporate and preserve high-resolution climate signals within their crystalline matrices, allowing modern interpretation of past climate systems (Holland et al., 1964; Hendy, 1971; Schwarcz et al., 1976; Gascoyne et al., 1980; Gascoyne, 1983; Schwarcz, 1986). Variations in speleothem $\delta^{18}O$ in caves with near 100% relative humidity (insignificant drip water evaporation $\delta^{18}O$ enrichment effects) and constant temperature (insignificant temperature-induced $\delta^{18}O$ variations) are most often interpreted as either changes in meteoric water sources (Bar-Matthews et al., 2003; Wang et al., 2001, 2008; Fleitmann et al., 2003b; Cruz et al., 2005a, 2007; Cobb et al., 2007), or changes in rainfall amount and intensity in monsoon climates (Burns et al., 2002; Fleitmann et al., 2003a; Cruz et al., 2005b; Johnson et al., 2006; Wang et al., 2005, 2008; Partin et al., 2007; Cheng et al., 2009).

Speleothem $\delta^{18}O$ records on glacial to interglacial time scales broadly covary with high-latitude solar insolation (Wang et al., 2004, 2008; Dykoski et al., 2005; Cheng et al., 2006, 2009), yet can deviate significantly from global insolation-based predictions over centuries or decades (Wang et al., 2008; Cheng et al., 2009) for reasons that are not well understood but are likely local or regional in scale. Recent studies have attempted to isolate the magnitude of these inter-dependent variables (Clemens et al., 2010; Dayem et al., 2010; Lambert and Aharon, 2010). Although many cave studies have described regional and global paleoclimate records, there have been few investigations of the relationships among drip water chemistry, cave air ventilation and the isotopic composition of modern calcite – what we call "modern calibration of speleothem paleoclimate proxies."

Oxygen isotopic fractionation in calcite is temperature dependent (Urey, 1948; McCrea, 1950; Epstein et al., 1951, 1953). Numerous laboratory-based inorganic calcite precipitation experiments have demonstrated a temperature-dependent oxygen isotopic fractionation from water to calcite of approximately $-0.23‰/°C$ (Epstein et al., 1953; O'Neil et al., 1969; Tarutani et al., 1969; Kim and O'Neil, 1997; Jimenez-Lopez et al., 2001). Laboratory calibrations at low temperatures (e.g., $T = 0$–40 °C) are challenging because it is difficult or impossible to demonstrate that precipitation of calcite occurs in oxygen isotope equilibrium with water (Coplen, 2007). There have been a few modern calibrations performed in the natural environment inside caves. *In situ* cave calibrations reveal that calcite $\delta^{18}O$ is "too high" ("too cold" or "too heavy") with respect to laboratory-based predictions (Desmarchelier et al., 2000; Plagnes et al., 2002; Genty et al., 2003; Genty, 2008; Mickler et al., 2004; Mangini et al., 2005; Guilfoyle, 2006; Coplen, 2007; Sinha et al., 2007; Boch, 2008; Boch et al., 2009). In order to correctly interpret local environmental changes in the past, it is necessary to understand the *in situ* conditions that alter annual banding and growth rates (Baker et al., 1993, 2008; Lachniet, 2009), such as seasonal cave ventilation (Pflitsch and Piasecki, 2003; Richon et al., 2005; Perrier et al., 2005; Spötl et al., 2005; Baldini et al., 2006b, 2008; Bourges et al., 2006; Kowalczk and Froelich, 2010), seasonal rainfall patterns and shifts in hydrology (Treble et al., 2003; Cruz et al., 2005b; Baldini et al., 2006a; Lambert and Aharon, 2010; Pape et al., 2010) and drip water chemistry (Spötl et al., 2005; Musgrove and Banner, 2004; Mickler et al., 2006; Guilfoyle, 2006; Banner et al., 2007; Tremaine, 2010; Wong et al., 2011).

To calculate paleotemperature (T) from calcite $\delta^{18}O$, knowledge of source water isotopic composition is necessary (O'Neil et al., 1969; Tarutani et al., 1969; Kim and O'Neil, 1997). To reduce errors associated with assuming the initial source water composition, fossil pore-water can be extracted from micro-inclusions and subjected to δD and $\delta^{18}O$ analyses (Schwarcz et al., 1976; Harmon et al., 1979; Winograd et al., 1992; Rowe et al., 1998; Matthews et al., 2000; Dennis et al., 2001; McGarry et al., 2004; Vonhof et al., 2006; van Breukelen et al., 2008; Zhang et al., 2008; Griffiths et al., 2010). However, this method is sensitive to oxygen isotope re-equilibration and requires specialized equipment. We are aware of only one study that attempts to replicate cave conditions in a laboratory setting – that of Day and Henderson (2011). Instead, we have measured rain and *in situ* temperature and drip water $\delta^{18}O$, cave air chemistry and isotopes (CO_2, ^{222}Rn, $\delta^{13}C$), and farmed calcite isotopes ($\delta^{18}O$ and $\delta^{13}C$) in a natural cave setting that we have been continuously monitoring for several years.

Speleothems form when high pCO_2 calcite-saturated drip waters degas, increasing pH and oversaturating the drip waters and leading to precipitation of calcite:

$$Ca^{2+} + 2HCO_3^- \rightarrow CaCO_3 + H_2O + CO_{2\,(g)} \uparrow \qquad (1.1)$$

Calcite $\delta^{13}C$ is often interpreted as a proxy for atmospheric CO_2 concentration (Baskaran and Krishnamurthy, 1993) and overhead vegetation composition (C3 vs. C4: Brook et al., 1990; Dorale et al., 1992; Bar-Matthews et al., 1997; Hou et al., 2003; Denniston et al., 2007). Until recently cave air and its CO_2 have been considered to be stagnant, i.e. with little or no air exchange with the atmosphere, fostering paleoclimate interpretations that focused only on atmospheric CO_2 and vegetation contributions to soil gas. Recent work has demonstrated that ventilation-driven outgassing of cave-air CO_2 must control drip water degassing of CO_2 and thus the rate and timing of calcite precipitation (McDermott, 2004; Mickler et al., 2004, 2006; Spötl et al., 2005; Bourges et al., 2006; Banner et al., 2007; Baldini et al., 2008; Kowalczk and Froelich, 2010) as well as the isotopic composition of drip water and subsequent calcite (Mattey et al., 2008; Cosford et al., 2009; Oster et al., 2010; Frisia et al., 2011; Lambert and Aharon, 2011). However, it is not yet clear how strong ventilation affects calcite $\delta^{18}O$ and $\delta^{13}C$ on seasonal, diurnal, and multi-decadal scales. The implication that all caves with calcite formation must breathe with outside air requires renewed evaluation of the effects of both CO_2-sources on ^{13}C, and temperature and evaporation effects on ^{18}O, a focus of this paper. The large number of dry caves in the northeast panhandle of Florida may be important for paleoclimate work because of a number of climatic factors.

Numerous studies have demonstrated a teleconnection between the sub-tropical Gulf of Mexico and high-latitude climate perturbations since the Last Glacial Maximum from marine forams in sediment cores (Poore et al., 2003, 2004, 2009; Richey et al., 2007, 2009; Ziegler et al., 2008), lake pollen records (Watts and Hansen, 1994; Willard et al., 2007), lake sediment records (Grimm et al., 1993, 2006; Mangini et al., 2007) and a few very limited speleothems records (Lachniet et al., 2004a,b; Mangini et al., 2007; van Beynen et al., 2007, 2008; Lambert, 2010). But the Southeast USA in general, and the Gulf Coast in particular, are notably lacking in high-resolution continental climate records such as those from speleothems (Lambert and Aharon, 2010). The most robust speleothem-derived paleoclimate records available are a few in which modern cave monitoring studies preceded investigation of fossil drip stones (Lambert and Aharon, 2011). We report here an extensive physical, chemical, and stable isotope data set designed to establish modern isotopic, temperature, ventilation and rainfall proxy calibrations with which to interpret paleoclimate records from ancient speleothems in north Florida.

2. STUDY SITE

Hollow Ridge Cave (HRC) is a wild, protected, phreatic-zone solution cave in Marianna, Florida, formed within the flat-lying Oligocene Marianna Limestone Formation, penetrating downward into the Bumpnose Limestone Formation. Hollow Ridge is hosted in the Chattahoochee Anticline and is an upland karst cave (normally dry), with unaltered entrances and few annual visitors. The cave is overlain by a thin soil veneer (average <30 cm thick) composed of Plio-Pleistocene sands and clays with multiple bedrock outcrops, and the vegetation is characterized as an "upland mixed forest" composed primarily of C3 trees and C4 shrubs and vines (Maddox, 1993). This cave is one of dozens of similar caves that occur in the tops of local ridges along the Chipola river, including the Florida Caverns public show cave.

Mean annual precipitation in Quincy, Florida (35 km east of Marianna, Florida) is approximately 1370 mm yr^{-1} (1984–2010; www.ncdc.noaa.gov), ranging from 917 mm (2007) to 2105 mm (1994). During this study, measured monthly rainfall at HRC ranged from 113 mm $month^{-1}$ (1356 mm from November 2007 to December 2008) to 123 mm $month^{-1}$ (1476 mm from December 2009 to January 2010). Mean annual atmospheric air temperature measured at HRC (2007–2010) was 18.3 °C, ranging from 8.57 °C (January 2008) to 26.6 °C (June 2009). The lowest elevation entrance to Hollow Ridge lies at approximately 21 m above sea level (ASL) at the edge of the flood plain of the Chipola river, which runs north-south approximately 400 m west of the study site. The highest entrance lies at 28 m ASL. The lowermost levels of the cave have experienced four river-flooding events in the past three years, events which block the lower entrances.

There are 1030 m of mapped passage within HRC (Fig. 1). The vertical throw between the lowest point (Ballroom) and the highest point (Signature Room) is 10 m, which is approximately the maximum overhead limestone thickness. Hollow Ridge passage is typically 1–2 m high, and floored by clay-mud up to 1 m thick. There is a vertical fissure that transects the cave from northwest to east-southeast, coinciding with the local limestone fault structure. The cave is owned, protected and managed by the Southeastern Cave Conservancy Inc. (SCCi). HRC is shallow and subject to large temperature gradients near the lower entrances and is thus not typical of larger deep caves which are often presumed to be at constant temperature and 100% relative humidity. Mean annual cave air temperatures measured continuously at two sites inside HRC (Fig. 1) were 18.8 °C (CS1) and 19.5 °C (CS2). However, winter airflow into Entrance-A and out Entrance-D (through-flow) can reduce in-cave air temperatures in the Entrance Room to approximately 12 °C. It is important to note that although HRC is an excellent cave in which to perform modern calibrations, temperature variations of this magnitude would require independent information for both H_2O–$\delta^{18}O$ and temperature for paleoclimate interpretations, and thus long-term speleothem records in the affected area near the entrance are only used here for calibration purposes. The deep interior of the cave (CS2), while ventilated (Kowalczk and Froelich, 2010), is much more stable.

We report here the second phase of an ongoing high-resolution time series cave-monitoring program that was established at Hollow Ridge Cave in November 2007 (Kowalczk, 2009). The primary goal of phase one was to instrument the cave for continuous monitoring and to investigate the rates and timing of cave ventilation. Three monitoring stations were deployed (Fig. 1): (1) an above ground micrometeorological (MET) station that records temperature (*T*), relative humidity (*RH*), barometric pressure (*BP*), wind velocity and direction, rainfall, and solar irradiance, all at 30-minute intervals; (2) an in-cave microchem station in the Entrance Room referred to as Cave Station 1 (CS1) that records *T*, *RH*, *BP*, Radon-222 (^{222}Rn), and air CO_2 concentration at one-hour intervals; and (3) a microchem station in the Signature Room referred to as Cave Station 2 (CS2) that records interior-cave *T*, *BP*, *RH*, ^{222}Rn and air CO_2 at one-hour intervals. Details of the instrumentation and methodology are reported in Kowalczk (2009) and Tremaine (2010).

We use Radon-222 (measured with portable Durridge RAD7's) as a cave air ventilation monitor to estimate rates at which HRC breathes with outside air (Kowalczk and Froelich, 2010). Radon-222 is a radioactive daughter of ^{226}Ra in the ^{238}U decay series and is constantly emitted from marine limestones. It is a heavy noble gas with very high aqueous solubility and serves as a non-reactive mass-transport proxy for CO_2 exchange on time scales less than five times its half-life ($t_{1/2} = 3.82$ days). Average atmospheric ^{222}Rn activity above HRC is effectively zero, measured at approximately 2 dpm L^{-1} on 11/10/2008, while cave air ^{222}Rn activities range from 50 to 100 dpm L^{-1} at CS1 and 65 to 400 dpm L^{-1} at CS2. Detectable atmospheric ^{222}Rn above HRC indicates that cave air is leaking upward through cracks in the cave ceiling, consistent with

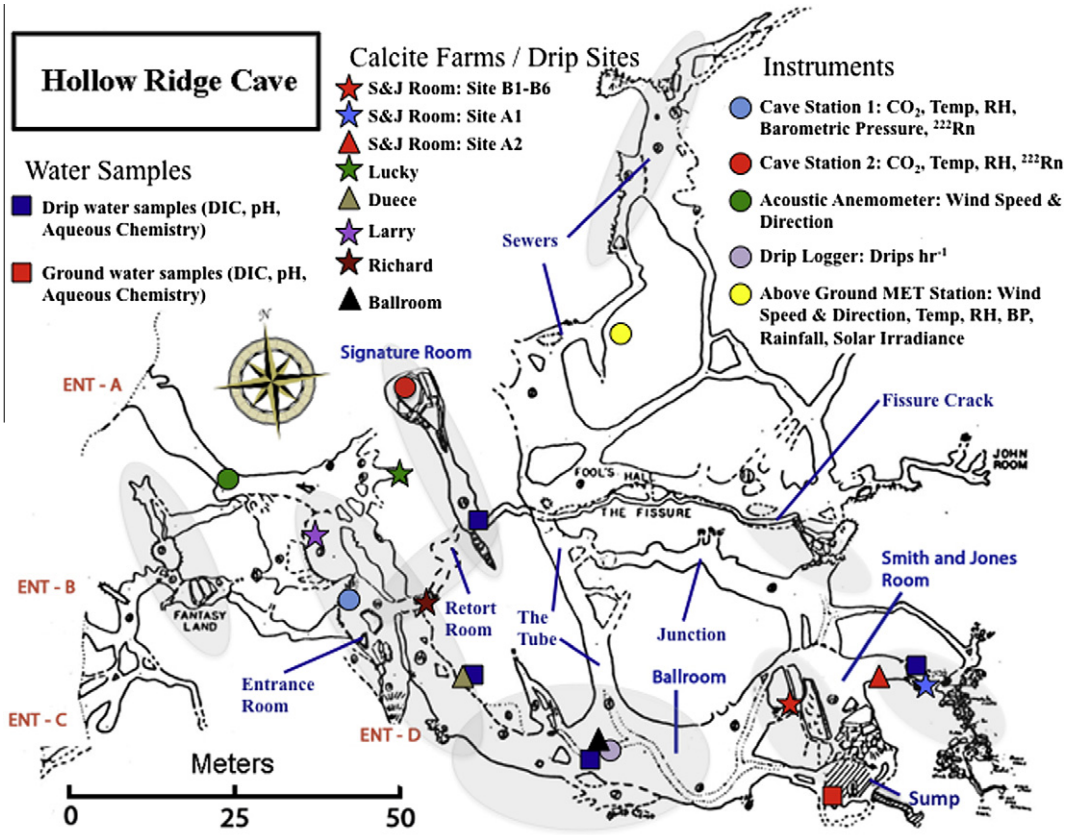

Fig. 1. Instrument, water samples and calcite farming locations. Plan view of HRC, Jackson County, FL (30°46′ 58.17″ N, 85° 12′ 13.15″ W, 21 m ASL). Continuous time series instrument groups are shown as colored circles (blue: Cave Station 1; red: Cave Station 2; green: Acoustic Anemometer; light purple: Drip Logger; yellow: Above Ground MET Station). Calcite farming locations are denoted by colored stars and triangles. Blue and red squares denote sites of drip and groundwater sampling for trace elements, δD and $\delta^{18}O$, major cations and anions, dissolved inorganic carbon ($TCO_2 = DIC = HCO_3^- + 2CO_3^{2-}$) and pH. Entrances A, B and C lie adjacent to the flood plain of the Chipola River (400 m west). Entrance D serves as the main entrance and is elevated 8 m from the other entrances. Shaded gray areas indicate the general locations of formations. Map adapted from Boyer (1975). Cave owned and managed by Southeastern Cave Conservancy Incorporated, PO Box 71857, Chattanooga, TN 37407-0857, Chairman: Brian Krebs; Cave Steward: Allen Mosler.

our understanding of the winter ventilation regime at HRC (warm air inside the cave is rising). Phase one data (2008–2009) were used to generate a ^{222}Rn deficiency model to estimate CO_2 outgassing as a function of cave-air ventilation rates, and seasonal calcite deposition based on net CO_2 export from Hollow Ridge Cave (Kowalczk and Froelich, 2010). In addition to chemical monitoring, an acoustic anemometer was deployed inside the cave at a restriction near the lower entrance (Fig. 1) to record cave air advection direction and velocity at one-hour intervals.

3. MATERIALS AND METHODS

3.1. Ventilation and cave air CO_2 and $\delta^{13}C$

To fill in longitudinal data between hourly time series data at CS1 and CS2, an additional portable Durridge RAD7 radon detector was carried through the cave bi-monthly in "snapshot mode" to grab air samples to determine the extent of ventilation in rooms and passages throughout the cave that were not being continuously monitored. Air samples were also collected bi-weekly under the forest canopy and from a soil flux chamber (soil-respired CO_2) installed atop the cave. Six in-cave air CO_2 grab sample transects were performed during the study, on 5/22/2009, 7/24/2009, 10/31/2009, 11/21/2009, 1/4/2010 and 2/28/2010. Each transect was completed in less than 2 h. Grab samples were compared with in-cave monitors (CO_2-Licor 820; ^{222}Rn-RAD7) to verify that cave ventilation conditions were stable during each transect. Grab air samples were drawn into a 60 mL syringe and injected into 30 mL evacuated glass vials sealed with rubber septa. Samples (150 μL) were analyzed for CO_2 concentration and $\delta^{13}C$ value on a *Finnigan* MAT V Delta Isotope Ratio Mass Spectrometer (IR-MS) at Florida State University (FSU) against internal standards (Electronic Annex (EA): Table EA.1) with typical 1σ analytical uncertainties of ±2.5 ppmv for CO_2 and ±0.39‰ for $\delta^{13}C$.

3.2. Drip and groundwater saturation state (Ω) and $\delta^{13}C$

To determine the calcite saturation state of drip and groundwaters, pH, $[Ca^{2+}]$, $[Mg^{2+}]$, and Total-CO_2

(TCO_2 = Total Dissolved Inorganic Carbon = DIC) were measured in waters collected at the same four locations monthly for four months (Ballroom, Duece, Smith and Jones A, Sump). Water pH was measured *in situ* with a Thermo Orion 210A pH meter and P9106 gel-filled semi-micro pH probe after in-cave calibration with pH-7 and pH-10 buffers. Multiple water samples were collected in 8 mL glass vials (TCO_2 and isotopes) and sealed with rubber septa. Vials were filled with fluid to avoid headspace equilibration with cave air and were kept cold and dark and analyzed within 24 h.

Samples for $\delta^{13}C$ and TCO_2 were treated with 0.5 mL of 105 % H_3PO_4, then shaken and pressurized with helium. Samples were allowed to equilibrate for 1 h, followed by injection of head-space air (150 μL) into a *Finnigan* MAT V Delta IR-MS coupled to a HP 5890 Series II Gas Chromatograph at FSU. Calibrations were performed at the beginning and end of each run using in-house standards (Table EA.1). The $\delta^{13}C$ (CO_2) values are reported in reference to the international VPDB scale as outlined by Coplen et al. (2006). Long-term reproducibility of the method is ±0.05‰ (1σ) for $\delta^{13}C$. TCO_2 and pH were used to calculate carbonate alkalinity and all other aqueous carbonate species using carbonate system constants at salinity (S) = 0‰ and temperatures of T_{cave} = 18 °C (Ballroom and Duece) and T_{cave} = 20 °C (Sump and Smith and Jones A) after Pilson (1998) (Fig. EA.1 and Table EA.2).

Unfiltered cation samples (Ca^{2+} and Mg^{2+}) were diluted to approximately 1 ppm [Ca] and measured on an *Agilent* Quadrupole 7500cs ICP-MS in 2 % *Optima*® HNO_3 spiked with 10 ppb Sc and 1 ppb Y internal standards following multiple-element standard-bracketing ICP-MS methods at FSU (methods modified from Yu et al., 2005). Calibration standards are shown in Table EA.1. See Tremaine (2010) for further details.

3.3. Drip and groundwater δD and $\delta^{18}O$

Drip and groundwater samples were collected bi-weekly for a period of 20 months from June 2008 through February 2010 at multiple sites throughout the cave, including the Ballroom (drip), Sump (ground), Duece (drip) and Smith and Jones Room A (drip) (Fig. 1). Water was collected unfiltered into 8-mL glass vials and sealed with rubber septa for isotope analyses. Vials were filled with fluid to avoid headspace equilibration with high CO_2 cave air. Monthly rain samples were also collected to provide local correlation. Drip water collection and sample preparation methods are described in Tremaine (2010). Samples (0.5 mL) were transferred by high-precision pipette into clean glass vials containing a platinum catalyst, capped and flushed with helium containing either 2% H_2 (for δD analyses) or 0.3% CO_2 (for $\delta^{18}O$ analyses), and then allowed to equilibrate isotopically for 24 h. Headspace gas was introduced via an on-line, continuous-flow system (*Finnigan* GasBench II) into a *Finnigan* MAT DELTA^{plus} XP IR-MS at FSU. For each sample, four reference gas measurements and 10 sample gas measurements were performed. Reported values are the average of 10 sample measurements. The data were calibrated based on measurements of interspersed sets (beginning, middle, end) of four different water isotope standards (Table EA.1) processed with each batch of samples and are reported as δD and $\delta^{18}O$ referenced to the international VSMOW scale. Calibration curves were anchored by ZNW-102 (δD = 4.93‰, $\delta^{18}O$ = 0.56‰ VSMOW). The 1σ analytical precision based on replicate analyses of lab standards processed with each batch of samples is ±0.1‰ or better for $\delta^{18}O$ and ±1‰ for δD.

3.4. Modern calcite farming and calcite $\delta^{18}O$ and $\delta^{13}C$

In November 2008 calcite "farming" was initiated under active drip sites in the Ballroom on standard glass microscope slides. Expansions of the farming project occurred in summer 2009, and again in fall 2009. Before deployment, slides were pre-weighed and then fixed tilted with a flexible wire mesh atop actively growing (dripping) stalagmites similar to the methods of Frisia et al. (2000), Mickler et al. (2004), Banner et al. (2007), and Boch et al. (2009) (Fig. EA.2). We did not attempt to attach seed crystals, so initial growth was undoubtedly delayed. After visual verification of calcite growth, slides were periodically removed and replaced. In this fashion, the farms were monitored for growth through seven three-month seasons. Recovered slides were rinsed with DDW, dried and weighed. Low-magnesium calcite growth was verified using visual microscopy of crystal habit and X-ray diffraction (Tremaine, 2010). No aragonite or vaterite were observed. Approximately 250-μg samples were removed from each plate into pre-cleaned glass vials and placed in an oven at 80 °C for 48 h to remove water. Vials were subsequently capped and flushed with helium and the samples acidified with 105% H_3PO_4, prepared following the standard procedure (Sharp, 2007), and left to react for 24 h at 25 °C. The resulting CO_2 was then introduced via an on-line, continuous-flow system (*Finnigan* GasBench II) into the IR-MS at FSU for isotopic analysis. The continuous flow method operates on the basis of identical treatment of standards and samples, resulting in identical acid fractionation factors (Werner and Brand, 2001; Paul and Skrzypek, 2007) which are inherently incorporated into our four-point calibration. Thus acid fractionation factors are not reported here although they can be calculated from the gas calibration data in Tremaine (2010).

Acid digestion of calcite standards and samples was performed at 25 °C, and the acid fractionation factor ($\alpha_{CO2(ACID)-CaCO3}$) was assumed to be 1.01030 (Kim et al., 2007). Reported values are the calibrated values of 10 replicate sample measurements. The $\delta^{13}C$ and $\delta^{18}O$ values were calibrated based on measurements of three sets each of four different carbonate standards (Table EA.1) processed with each batch of samples and are reported in reference to the international carbonate VPDB scale. Calibration scales were anchored with NBS-19 ($\delta^{18}O$ = −2.20‰, $\delta^{13}C$ = +1.95‰ VPDB) as outlined in Coplen (1996). The analytical precision (based on replicate analyses of lab standards processed with each batch of samples) is ±0.1‰ (1σ) or better for both $\delta^{13}C$ and $\delta^{18}O$.

4. RESULTS

4.1. Seasonal ventilation regimes

Hollow Ridge Cave experiences diurnal ventilation driven by two distinct regimes: winter and summer (Kowalczk and Froelich, 2010) (Fig. 2). During the winter, cold, dry and dense air enters the bottom of HRC through Entrance A and is moisturized and convectively heated by cave walls, becoming more buoyant and rising to exit through cracks in the cave ceiling at the east end of the cave. The air is accelerated through relatively small openings at the top of the cave (a "ceiling leak") creating a pressure differential, which in turn draws more dense cold air into the bottom of the cave through Entrance A at up to 1.2 m s^{-1} (Fig. 2). These types of "ceiling leak" ventilation pathways are undiscoverable without detailed in-cave and atop-cave ^{222}Rn snooping. This style of ventilation results in near-atmospheric levels of CO_2 (385–450 ppmv) and relatively low levels of ^{222}Rn activity (40–120 dpm L^{-1}) in the ventilation flow path. Winter air is cooler than the cave at night and can often becomes warmer during the day. Because cave wall temperatures are virtually constant, the system can switch back and forth diurnally from inflow at entrance-A and outflow through the ceiling leaks late at night (20:00–09:00 h) to stagnant or sluggish inflow at the ceiling leak and outflow at entrance-A during day-time heating (10:00–18:00 h).

In the summer, outside air temperatures rise rapidly after sunrise (07:00 h) from approximately 20 °C to 35 °C. Convective cooling then induces down-drafting through the same small openings in the top of the cave. Atmospheric air (warmer than cave-air) is entrained downward through the ceiling leaks, becoming cooler and increasingly more dense from interaction with cave walls. Similar to the winter ventilation regime, the cave walls impart moisture to summer air (which is already fairly high water content), decreasing the density contrast. The downward velocity of the entrained air mass is reduced by this added buoyancy, resulting in flow velocities out of Entrance A of less than 0.4 m s^{-1} (Fig. 2). Due to slower summer air advection and increased soil gas CO_2 production, summer time cave-air CO_2 and ^{222}Rn levels are elevated and often display periods of stagnation with little to no ventilation.

During spring and autumn ventilation, evening outside air temperatures are slightly cooler than the cave, often resulting in inflow at Entrance A. Daytime temperatures are warmer than the cave, resulting in downdraft through the ceiling leak and outflow through Entrance A. During these "change" seasons, HRC experiences a bimodal diurnal flow with an equal amount of inflow and outflow. When outside air densities are identical to cave wall temperatures, ventilation slows dramatically and the cave experiences 'stagnation'. Thus, spring and fall ventilation regimes are characterized by morning inflow, a period of stagnation,

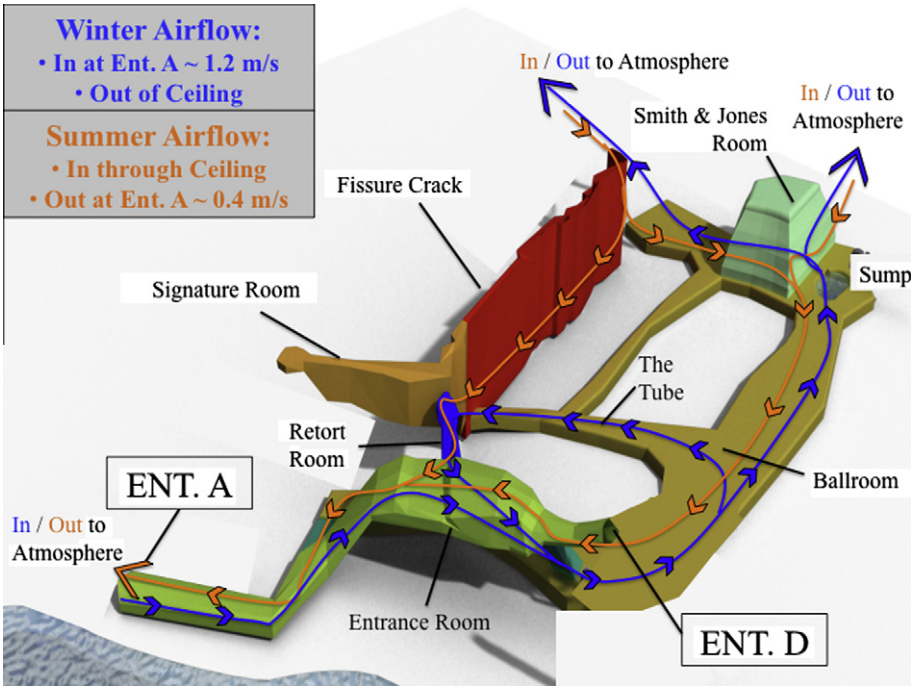

Fig. 2. Schematic cartoon of ventilation pathways in Hollow Ridge Cave. Dense (cold and dry) winter air (blue lines) flows into Entrance A and is convectively warmed and moistened as it travels upward through the Ballroom, Sump, and Smith and Jones Room and out of the top of the cave near the Fissure Crack. Air also travels through the Tube and is cycled through the Retort Room, back through the Entrance Room and into the Ballroom. Buoyant (warm and wet) summer air (orange lines) flows in the top of the cave and is convectively cooled as it travels downward in two paths: (1) through the Fissure Crack, Retort Room and out through Entrance A, and (2) through the Smith and Jones Room, Sump, Ballroom and the Throat leaving Entrance A. Calcite growth rates at Smith and Jones farming locations also indicate that atmospheric air is entrained through cracks in the eastern edge of the cave. Figure presented with permission from D. Nof, FSU.

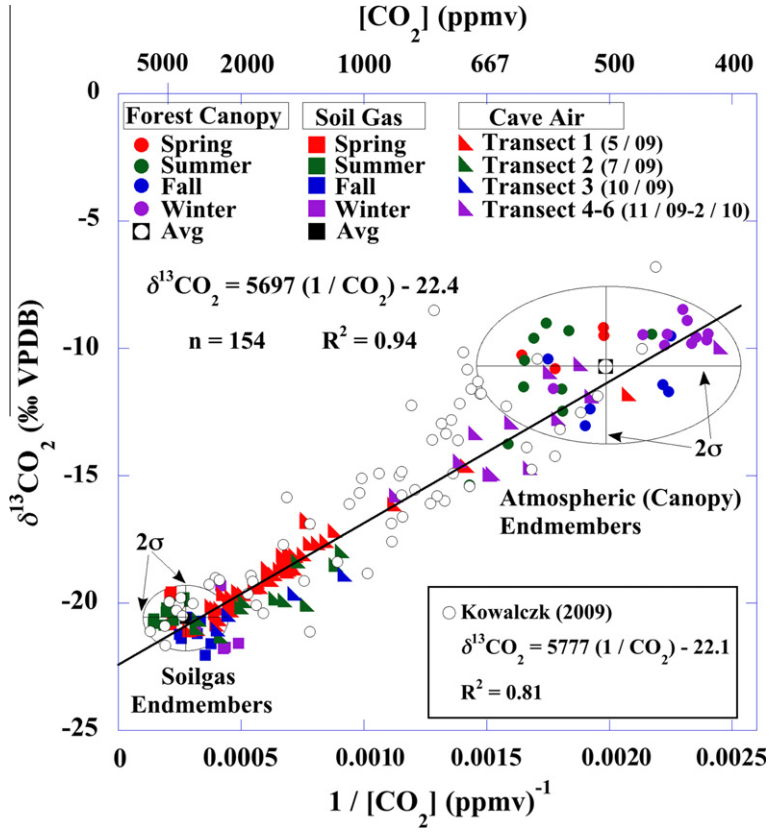

Fig. 3. Keeling plot of Hollow Ridge Cave air samples. Colored solid circles denote atmospheric samples above cave (free air under tree canopy). Colored solid squares represent seasonal soil gas samples. Triangles denote in-cave air transect snapshots. Each endmember average (atmosphere and soil gas) is circumscribed by a $\pm 2\sigma$ (range) oval. The best-fit line includes soil gas, atmospheric and in-cave samples from the current study but does not include Kowalczk (2009) samples (black circles), although a line through the in-cave transect snapshot data only is nearly identical. The equation describing the best-fit line ($\delta^{13}C = 5697/CO_2 - 22.4$, $R^2 = 0.94$) indicates that the isotopic composition of HRC air is a function of mixing in a two-endmember system (soil gas and atmosphere). The endmember values for soil and air are expanded in Fig. 4.

and afternoon outflow through the lower entrances. Spring and fall ventilation results in high-amplitude diurnal variation in cave air CO_2 and ^{222}Rn (Kowalczk and Froelich, 2010). Prolonged periods of stagnation were observed when Chipola River flooding events seal off the lower entrances of HRC, eliminating ventilation altogether. The highest ^{222}Rn activity (1200 dpm L^{-1}) and ingrowth rates (40 dpm L^{-1} h^{-1}) were measured during these flooding events (Kowalczk, 2009; Tremaine, 2010).

4.2. Cave air CO_2 and calcite growth rates

Kowalczk and Froelich (2010) observed a ventilation-driven mixing relationship between cave air CO_2 and $\delta^{13}C$ in HRC that follows the Keeling relationship (Keeling, 1958). They found that the average soil gas CO_2 endmember ($\delta^{13}C = -20.7‰$ at 4077 ppmv) mixes with 'outside' (under canopy) air CO_2 ($\delta^{13}C = -10.7‰$ at 513 ppmv) to produce ventilation gradients inside the cave. A soil gas endmember of $\delta^{13}C = -20.7‰$ requires a 35% contribution of C4 plant respiration and a 65% C3 tree respiration (assuming $\delta^{13}C = -11‰$ and $-26‰$ for C4 and C3, respectively), which is typical for a "mixed upland forest" (Maddox, 1993). Following the protocol established in Kowalczk (2009), high-resolution bi-weekly samples of atmospheric, soil gas, and cave-air CO_2 and $\delta^{13}C$ were collected. New data from the present study were then plotted with data from Kowalczk and Froelich (2010) (Fig. 3). The best-fit line through in-cave air grab samples extends directly through both endmember averages indicating that CO_2 concentrations in cave air and $\delta^{13}CO_{2\ cave\ air}$ represent a ventilation-driven mixture between only two endmembers: soil gas and outside atmosphere. The significance of this cave air mixing relationship in Fig. 3 is that stalagmites and their drip solutions at fixed locations inside a cave are experiencing a range of both CO_2 and ^{13}C depending on proximity to the cave entrance or cave interior *and* the ventilation regime that are being seasonally modulated (direction of flow and turbulence).

4.2.1. *Atmospheric (under canopy) air CO_2 seasonality*

CO_2 endmembers in Fig. 3 are expanded in Fig. 4 to demonstrate seasonal cycles in soil gas and canopy air.

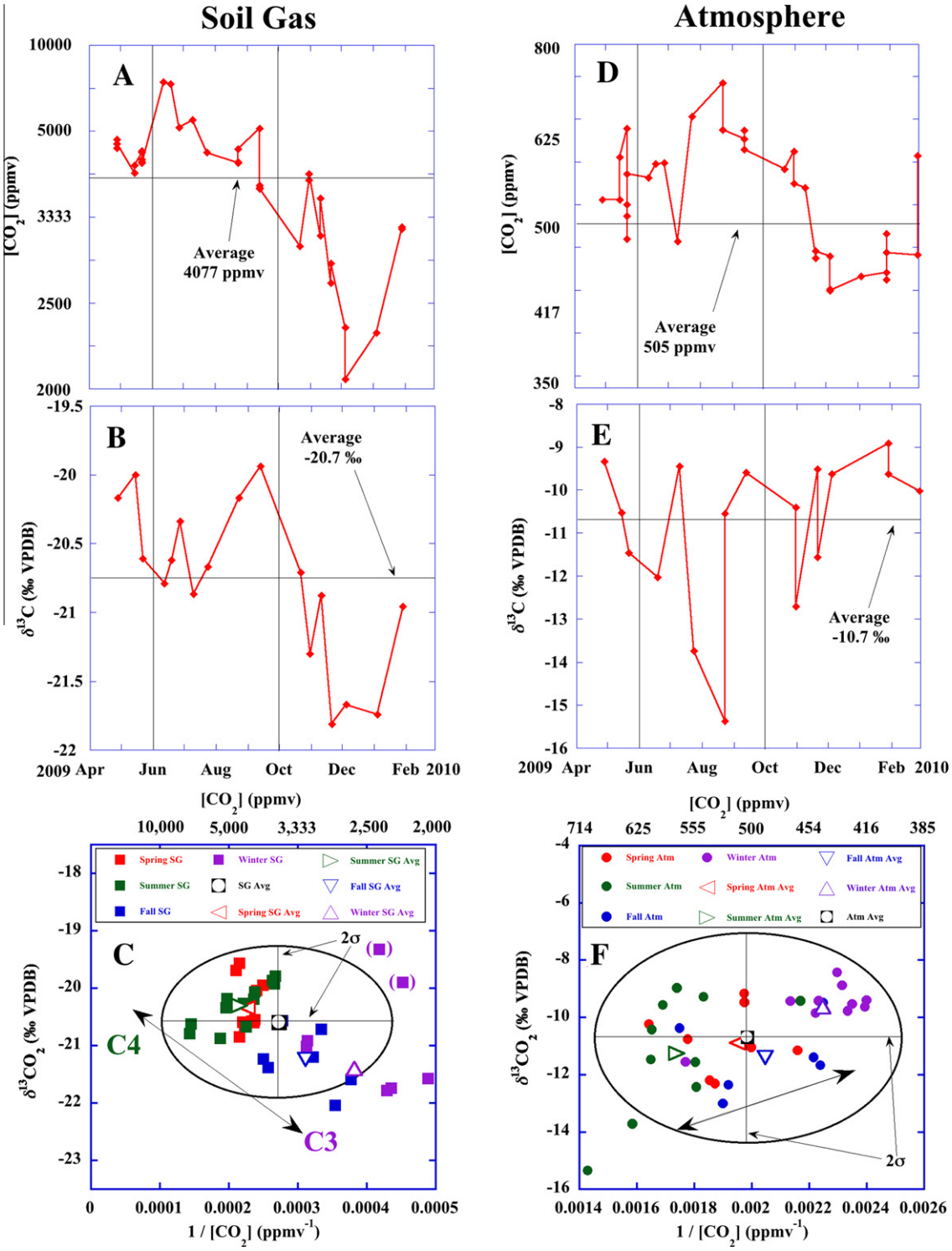

Fig. 4. Seasonal cycles of soil gas and atmospheric CO_2 endmembers. (A) Soil gas [CO_2] time series from April 2009 to February 2010. (B) Soil gas $\delta^{13}C$ time series from April 2009 through February 2010. (C) Keeling plot of soil gas endmember; $\delta^{13}CO_2$ vs. 1/[CO_2]. (D) Under canopy [CO_2] time series from April 2009 to February 2010. (E) Atmospheric $\delta^{13}C$ time series from April 2009 through February 2010. (F) Keeling plot of atmospheric endmember; $\delta^{13}CO_2$ vs. 1/[CO_2]. (A and D) were generated as inverse (1/[CO_2]) and plotted as a linear [CO_2] y-axis. Filled circles and squares in (C and F) are the same as in Fig. 3. Open triangles represent seasonal averages of data with corresponding colors. Parentheses around two data points in (C) signify data that are believed to have been improperly sampled and are not included in the average. Double-ended arrows in (C and F) indicate the vectors along which seasonal shifts occur in endmember values. Soil gas (C) shifts from higher $\delta^{13}C$ and high pCO_2 to lower $\delta^{13}C$ and less concentrated CO_2 as plant populations change from summer (C4 and C3) to winter (C3 only) (Ehleringer et al., 1997). Atmospheric gas (F) shifts from higher $\delta^{13}C$ and lower CO_2 concentration in the winter to lower $\delta^{13}C$ and higher CO_2 concentrations in the summer. The atmospheric shift indicates that air trapped between the tree canopy and the cave exhibits simple mixing between atmosphere (−8‰, 390 ppmv) and soil gas (−20.7 ± 0.66‰ (1σ range), 4077 ppmv).

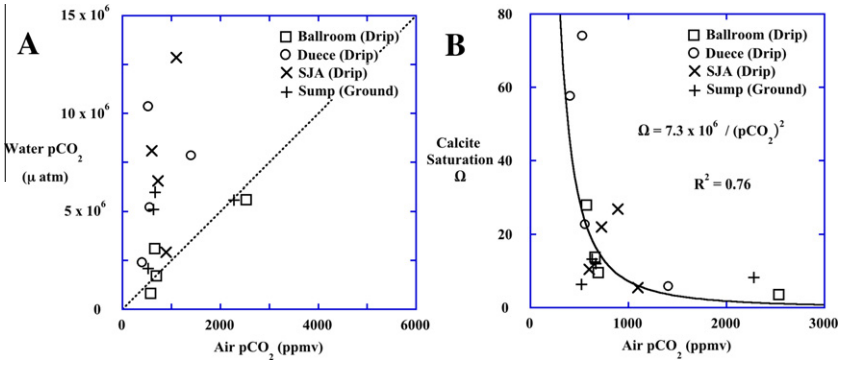

Fig. 5. Water pCO_2 and Calcite Saturation (Ω) as a Function of Cave Air pCO_2. (A) Cave Air pCO_2 (measured) vs. Water pCO_2 (calculated) of drip and groundwaters at the same four sites for four months (10/31/2009, 11/21/2009, 1/4/2010, 2/28/2010); Ballroom, Duece, Smith and Jones Room A, and Sump. The black dotted line represents the 1:1 CO_2 partitioning ratio expected when CO_2 in drip water is in chemical equilibrium with CO_2 in cave air. In general Ballroom drips exhibit equilibrium values. Duece, Smith and Jones A and Sump water pCO_2 values are above the line, which indicates that they were still degassing at the time of sampling. (B) Measured Cave Air pCO_2 vs. Calculated Calcite Saturation (Ω). The best-fit line suggests a hyperbolic relationship between air pCO_2 and calcite saturation of the equation: $\Omega = 7.3 \times 10^6/(pCO_2)^2$. The line indicates that Ballroom, Duece, and Smith and Jones drip waters will become unsaturated ($\Omega < 1$) at air $pCO_2 > 2500$ ppmv, but will become supersaturated at pCO_2 values below approximately 700 ppmv. Example calculations of water pCO_2 and Ω are shown in the electronic annex (*Table* EA.2).

Atmospheric air samples collected above the cave and under the forest canopy (Fig. 4D through F) exhibit the least depleted $\delta^{13}CO_2$ (−9.6‰) and lowest pCO_2 (440 ppmv) in the winter, a slightly more depleted $\delta^{13}CO_2$ (−11.4‰) and higher pCO_2 (500 ppmv) in fall and spring $\delta^{13}CO_2$ (−10.8‰), and highest CO_2 (575 ppmv) ($\delta^{13}CO_2 = -11.3$‰) concentrations during summer. The linear trend in average values from low pCO_2-high $\delta^{13}CO_2$ (winter) to high pCO_2-low $\delta^{13}CO_2$ (summer) falls on the extended mixing line in Fig. 3, and reveals that 'under canopy' atmospheric air samples represent a mixture of soil gas (ventilated from soils and from inside the cave) and true "free" tropospheric air above the canopy ($\delta^{13}CO_2 = -8$‰ at 390 ppmv) (Fig. 4F). During the winter, soil temperatures decrease, and soil gas diminishes, reducing the CO_2 flux into the understory. In addition as deciduous trees shed some of their leaves, a higher percentage of "free" atmosphere mixes into the understory.

4.2.2. Soil gas CO_2 seasonality

Soil gas exhibits the most depleted $\delta^{13}CO_2$ (−21.5‰) and lowest pCO_2 (2600 ppmv) during the winter, with less depleted $\delta^{13}CO_2$ (−21‰) and higher pCO_2 (3300 ppmv) in fall, and the highest pCO_2 (4700 ppmv) and least depleted $\delta^{13}CO_2$ (−20.3‰) in spring and summer (Fig. 4C). The average seasonal values trend from low pCO_2-low $\delta^{13}CO_2$ (winter) to high pCO_2-high $\delta^{13}CO_2$ (summer), orthogonal to an extension of the cave air mixing line. This trend suggests that plant root respiration is highest in the spring and summer (high CO_2), and that the C4 plant productivity (respired $\delta^{13}CO_2 = -11$ to −14‰ VPDB) is higher in the warmer months resulting in ^{13}C-enriched soil gas (Ehleringer et al., 1997). This soil gas seasonal cycle was not observed in cave air.

One of the fundamental questions in speleothem-based paleoclimate studies involves whether high temporal resolution geochemical signals of seasons are preserved in ancient calcite. Results from this study show that summer calcite growth in the interior of Hollow Ridge Cave is one to two orders of magnitude slower than growth at the same locations in fall, spring and winter (Table EA.3). These results support the hypothesis that slower summer ventilation rates result in elevated cave-air CO_2, which in turn slows drip water CO_2 degassing rates and thus speleothem precipitation rates. Ancient speleothems far from the entrances in Hollow Ridge Cave do not precipitate enough calcite during the summer to allow seasonal resolution of trace element and isotopic records. Therefore, we predict that paleoclimate interpretations from Hollow Ridge Cave stalagmites will be more reflective of winter and fall conditions, which could alias annual interpretations.

4.3. Drip water chemistry and calcite saturation state (Ω)

Calcite precipitation rate is expected to be directly proportional to drip water oversaturation ($\Omega > 1$) (Teng et al., 2000; De Yoreo et al., 2009). To establish the relationship between ventilation and saturation state (precipitation rate), drip and groundwaters were analyzed throughout a 4-month study from 10/31/2009 to 2/28/2010 (Table EA.4). Drip and groundwaters were both always supersaturated with respect to calcite ($\Omega_{Range} = 3.6$–73). Our aqueous chemistry data are typical of data from other caves. TCO_2, pH, $\delta^{13}C$, $[Ca^{2+}]$, $[Mg^{2+}]$, and calcite saturation state were similar to cave waters measured by Plummer et al. (2000), Mickler et al. (2004), Spötl et al. (2005), Banner et al. (2007), and Lambert and Aharon (2011) (Table EA.5). Ballroom drip water samples were found to be in chemical equilibrium with cave air CO_2, while Duece, Smith and Jones A and the Sump were still degassing at the time of sampling (Fig. 5A). If drip water

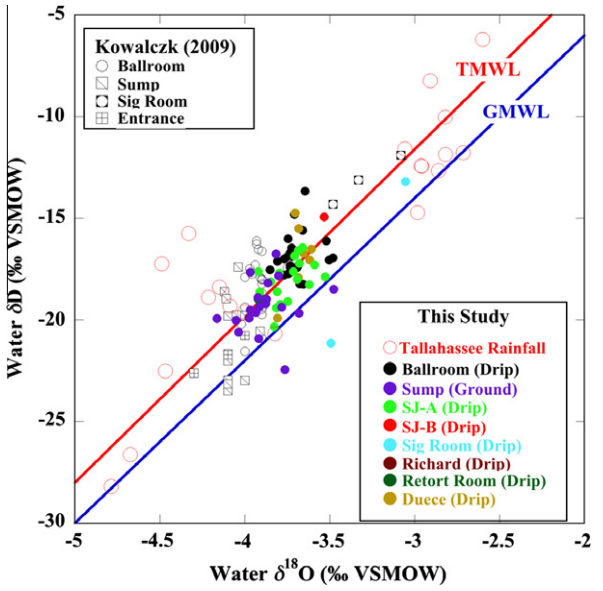

Fig. 6. Tallahassee Rainfall and Hollow Ridge Cave Drip water and Groundwater δD vs. $\delta^{18}O$ (‰ VSMOW) plotted with Global Meteoric Water Line (GMWL – blue line; $\delta D = 8{\cdot}\delta^{18}O + 10$; Craig, 1961; Dansgaard, 1964) and the Tallahassee Meteoric Water Line (TMWL – red line; $\delta D = 8.2{\cdot}\delta^{18}O + 13$). Red open circles designate Tallahassee Rainfall. Black open circles and squares represent data from Kowalczk (2009) from April 2008 to January 2009. Colored circles are cave data from the current study (January 2009 to February 2010). Cave water samples exhibit much less variation than rain samples, indicating water homogenization in the epikarst reservoir and phreatic zone.

$CO_{2\ (aq)}$ is in chemical equilibrium with cave air $CO_{2\ (g)}$ then the saturation state of water (Ω) with respect to calcite (after impingement upon a speleothem) should be a function of cave air CO_2 on timescales of seconds (Zeebe et al., 1999; Schulz et al., 2006; Dreybrodt and Scholz, 2011). Indeed, we find a hyperbolic relationship between cave air pCO_2 and drip water saturation state (Fig. 5B) described by:

$$\Omega = 7.3 \times 10^6/(pCO_2)^2 \quad R^2 = 0.76 \qquad (4.3.1)$$

Although this experiment was relatively short and should be repeated over several seasons, this relationship reveals that drip water saturation state (and therefore precipitation rate) increases rapidly below cave air pCO_2 values of approximately 700 ppmv (Fig. 5). Eq. (4.3.1) can be used to predict drip water saturation state as a continuous function of cave air pCO_2, which is a potential predictive tool when coupled with pCO_2 time series. Summer cave-air pCO_2 inside HRC averages approximately 1084 ppmv while winter cave-air pCO_2 averages 445 ppmv (Tremaine, 2010). These findings are consistent with the hypothesis that slower summer time ventilation in HRC leads to high cave air CO_2 that greatly reduces calcite precipitation rates. Example calculations are shown in Table EA.2.

4.4. Rainfall and drip water $\delta^{18}O$ & δD

Rain water was collected monthly and the amount-weighted average of Tallahassee rainfall $\delta^{18}O$ during this study period (February 2009 to February 2010) was $-3.56 \pm 1.18‰$ (2σ range) (Fig. 6). Hollow Ridge drip water $\delta^{18}O$ during this study ranged from $-3.05‰$ to $-4.16‰$ with an average of $-3.75 \pm 0.33‰$ (2σ range) (Fig. 6). Tropical Storm Fay (August 22nd, 2008) delivered approximately 80 mm of isotopically light rain ($\delta^{18}O = -14‰$ VSMOW) to Marianna, Florida. However, this excursion was not observed in drip waters (Kowalczk, 2009, his Fig. 4.14). Limited $\delta^{18}O$ variability of cave drips indicates that the epikarst-storage reservoir is relatively large and its water residence time sufficiently long (at least 2 weeks) to homogenize the isotopic composition of drips. This limited range in drip water $\delta^{18}O$ simplifies calculation of temperatures based on water–calcite oxygen isotopic fractionation (Lachniet, 2009).

4.5. Predicted and measured calcite $\delta^{18}O$

Farming modern calcite under drips of known isotopic composition in a cave that is well-monitored for temperature and ventilation is essentially a "natural laboratory" (Poulson and White, 1969; Coplen, 2007) that allows calibration of the temperature-dependence on speleothem calcite $\delta^{18}O$ ($\Delta\delta^{18}O_{CaCO3}/\Delta T$). We will consider that only evaporation, temperature, and drip water $\delta^{18}O$ variation can have significant impact on *in situ* calcite $\delta^{18}O$ assuming that calcite forms very close to oxygen isotopic equilibrium with drip water. The oxygen atom content of water is ~55 molar while HCO_3^- is in the 1–3 mM range and thus DIC-water oxygen isotope exchange should control the bulk isotopic composition of the carbonic acid system (O'Neil and Truesdell, 1991; Kim and O'Neil, 1997). Cave air relative humidity in the interior of HRC is always 97–100% (Tremaine, 2010), which minimizes the effects of evaporation and reduces calcite $\delta^{18}O$ composition to a function of drip water isotopic composition ($\delta^{18}O = -3.75 \pm 0.33‰$) and formation temperature (T). Measured atmospheric (MET station directly atop Hollow Ridge Cave – Fig. 1) and cave air temperatures (CS1 and CS2) combined with in-cave transects allows estimation of air temperatures at each farming location to within ±0.5 °C.

Measured $\delta^{18}O$ values of drip water and *in situ* temperatures were used to calculate predicted calcite $\delta^{18}O$ values based on both the O'Neil et al. (1969) equation (Eq. (4.5.1)) and the Kim and O'Neil (1997) equation (Eq. (4.5.2)) (data are in Table 1). The O'Neil et al. (1969) equation, as modified by Friedman and O'Neil (1977) and hereafter referred to as O'Neil et al. (1969), is based on extrapolation from their high-temperature (250–700 °C) fractionation line through two low-temperature experimental data points (0 and 25 °C), thus having the form $10^6\ T^{-2}$. The Kim and O'Neil (1997) equation, as modified by Kim et al. (2007) and hereafter referred to as Kim and O'Neil (1997), is based on low-temperature (10–40 °C) experimental calcite precipitation and has the form of $10^3\ T^{-1}$.

Table 1
Predicted and measured calcite $\delta^{18}O$ values. Predicted values based on drip water $\delta^{18}O$ of $-3.75 \pm 0.33‰$ (2σ) (VSMOW) (Tremaine, 2010). Measured calcite values represent the average value for each location during that growing season. Averages were calculated as $\Sigma\delta^{18}O/n$ where n is the number of individual analyses.

Calcite farming location	Temperature (°C)	This study (measured) $\delta^{18}O$ ‰ (VPDB)	Predicted from Kim and O'Neil (1997)[a] $\delta^{18}O$ ‰ (VPDB)	Predicted from O'Neil et al. (1969)[b] $\delta^{18}O$ ‰ (VPDB)	Predicted from Chacko and Deines (2008)[c] $\delta^{18}O$ ‰ (VPDB)	Predicted from Horita and Clayton (2007)[d] $\delta^{18}O$ ‰ (VPDB)
Summer						
Larry	21.5		−5.09	−4.97	−5.26	−5.39
Duece	20.5	−3.57	−4.88	−4.76	−5.16	−5.19
Smith Jones A-l	19.5	−4.07	−4.67	−4.54	−4.96	−4.98
Smith Jones A-2	19.5		−4.67	−4.54	−4.96	−4.98
Ballroom	20.5		−4.88	−4.76	−5.16	−5.19
Lucky	19.2	−3.88	−4.61	−4.47	−4.90	−4.91
Smith Jones B	19.7	−4.08	−4.71	−4.58	−5.00	−5.02
Richard	21.5	−4.02	−5.09	−4.97	−5.26	−5.39
Fall						
Larry	16.0		−3.93	−3.75	−4.23	−4.23
Duece	18.5	−3.41	−4.46	−4.31	−4.76	−4.77
Smith Jones A-l	20.0		−4.77	−4.65	−5.06	−5.08
Smith Jones A-2	20.0		−4.77	−4.65	−5.06	−5.08
Ballroom	19.5	−3.94	−4.67	−4.54	−4.96	−4.98
Lucky	19.2	−3.78	−4.61	−4.47	−4.96	−4.91
Smith Jones B	20.0		−4.77	−4.65	−5.06	−5.08
Richard	21.0	−4.23	−4.98	−4.87	−5.26	−5.29
Winter						
Larry	12.0	−2.16	−3.05	−2.81	−3.37	−3.35
Duece	18.0	−3.41	−4.35	−4.20	−4.65	−4.66
Smith Jones A-l	19.2	−3.98	−4.61	−4.47	−4.90	−4.91
Smith Jones A-2	19.2	−4.06	−4.61	−4.47	−4.90	−4.91
Ballroom	18.0	−3.46	−4.35	−4.20	−4.65	−4.66
Lucky	19.2	−3.69	−4.61	−4.47	−4.90	−4.91
Smith Jones B	19.2	−3.91	−4.61	−4.47	−4.90	−4.91
Richard	21.0	−4.31	−4.98	−4.87	−5.26	−5.29
Spring						
Larry	16.0	−2.86	−3.93	−3.75	−4.23	−4.23
Duece	18.5	−3.74	−4.46	−4.31	−4.76	−4.77
Smith Jones A-l	20.0	−3.91	−4.77	−4.65	−5.06	−5.08
Smith Jones A-2	20.0	−4.35	−4.77	−4.65	−5.06	−5.08
Ballroom	19.5		−4.67	−4.54	−4.96	−4.98
Lucky	19.2		−4.61	−4.47	−4.90	−4.91
Smith Jones B	20.0		−4.77	−4.65	−5.06	−5.08
Richard	21.0	−3.83	−4.98	−4.87	−5.26	−5.29

[a] As modified by Kim et al. (2007) temperature equation: $1000 \ln \alpha = 18.03 (10^3/T) - 31.17$.
[b] As modified by Friedman and O'Neil (1977) temperature equation: $1000 \ln \alpha = 2.78 (10^6/T^2) - 2.89$.
[c] Chacko and Deines (2008) temperature equation was constructed by us from their published reduced partition coefficient data as: $1000 \ln \alpha = 2.5733 (10^6/T^2) - 0.869$.
[d] Horita and Clayton (2007) temperature equation: $1000 \ln \alpha = 0.9521 (10^6/T^2) + 11.59 (10^3/T) - 21.56$.

$$1000 \ln \alpha = \frac{2.78(10^6)}{T^2} - 2.89 \quad (4.5.1)$$

O'Neil et al. (1969), Friedman and O'Neil (1977)

$$1000 \ln \alpha = \frac{18.03(10^3)}{T} - 32.17 \quad (4.5.2)$$

Kim and O'Neil (1997), Kim et al. (2007).

$$\alpha = \alpha_{CaCO_3-H_2O} = \frac{1000 + \delta_{CaCO_3}}{1000 + \delta_{H_2O}} \quad (4.5.3)$$

$$\Delta\delta^{18}O\ CaCO_3/\Delta T = -0.206‰/°C \quad \text{Kim and O'Neil (1997)} \quad (4.5.4)$$

T = Kelvin.

Predicted calcite $\delta^{18}O$ values were then compared to measured calcite $\delta^{18}O$ values. Measured farmed calcite $\delta^{18}O$ values are consistently offset from predicted values by:

Authors	Offset (‰ VPDB)
Kim and O'Neil (1997)	0.82 ± 0.22
O'Neil et al. (1969)	0.68 ± 0.22
Chacko and Deines (2008)	1.11 ± 0.22
Horita and Clayton (2007)	1.13 ± 0.22

Hollow Ridge Cave calcite is more enriched in ^{18}O than predicted by Kim and O'Neil (1997) for their 5 mmol initial $[Ca^{2+}]$ solution, which they interpreted as "the slowest" kinetics and thus closest to isotopic equilibrium (Fig. 7). Note that the $[Ca^{2+}]$ concentrations in HRC drips are 0.7–1.8 mmol. Speleothem studies at different latitudes, altitudes, and temperatures have reported similar "too high" offsets (Desmarchelier et al., 2000; Plagnes et al., 2002; Genty et al., 2003; Mickler et al., 2004, 2006; Coplen, 2007; Sinha et al., 2007; Boch et al., 2009) as summarized and discussed by McDermott et al. (2006). Additionally, fluid inclusion investigations have revealed corresponding offsets (McDermott et al., 2006; van Breukelen et al.,

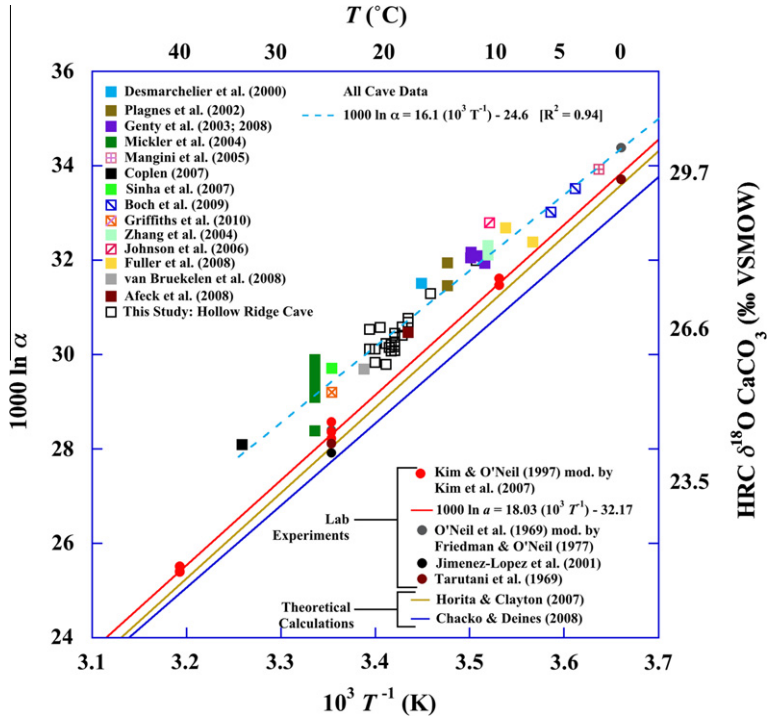

Fig. 7. 1000 ln α vs. $10^3\ T^{-1}$ For Calcite from Laboratory, Theoretical, and Cave Studies where the right y-axis is HRC calcite $\delta^{18}O$ (VSMOW), and the top x-axis is temperature (°C) plotted for Hollow Ridge Cave calcite (black open squares). HRC data shown are average values for each farming site by season. Other modern cave studies (solid and crossed squares), laboratory-based inorganic precipitation values (circles), and theoretical calculations (lines) are reported from those studies that reported calcite $\delta^{18}O$–H_2O data. The red line is the best-fit line from Kim and O'Neil (1997) as modified by Kim et al. (2007): 5 mmol L^{-1} $[Ca^{2+}]$ (red filled circles) where 1000 ln $\alpha = 18.03\ (10^3\ T^{-1}) - 32.17$. Not shown are Kim and O'Neil (1997): 15 mmol L^{-1} $[Ca^{2+}]$ where 1000 ln $\alpha = 21.69\ (10^3\ T^{-1}) - 43.55$; and 25 mmol L^{-1} $[Ca^{2+}]$ where 1000 ln $\alpha = 21.56\ (10^3\ T^{-1}) - 42.55$. Hollow Ridge Cave drip samples ranged from 0.6 to 1.8 mmol L^{-1} $[Ca^{2+}]$ and average drip $\delta^{18}O$ was $-3.75 \pm 0.33‰$ (2σ range) (VSMOW). The light-blue dashed line through cave data is the linear best-fit line 1000 ln $\alpha = [16.1 \pm 0.65]\ (10^3\ T^{-1}) - [24.6 \pm 2.2]$ (98% C.I.) ($R^2 = 0.94$) for all cave deposits. This result is significantly different from Kim and O'Neil (1997) 5 mmol data line at the 98% confidence interval. Equations for theoretical calculations are shown in *Table* EA.6. Analytical uncertainty for single measurements during the Hollow Ridge Cave study was less than 0.14‰ (1σ). 1000 ln $\alpha = 1000 * \ln[(1000 + \delta^{18}O_{Calcite})/(1000 + \delta^{18}O_{Drip\ H2O})]$ where for HRC $\delta^{18}O_{Drip\ H2O} = -3.75 \pm 0.33‰$ (VSMOW).

2008; Zhang et al., 2008; Griffiths et al., 2010). Authors of cave studies often state that their calcite was precipitated *at or approaching* equilibrium with water $\delta^{18}O$, statements that are virtually unprovable.

Coplen (2007) defended that Devil's Hole submerged vein calcite (enriched in $\delta^{18}O$ by 1.5‰ over that predicted by Kim and O'Neil, 1997 at 33.7 °C) had precipitated in isotopic equilibrium by proving that: (1) there is <0.2‰ variation along the axis of the vein calcite $\delta^{18}O$ (sample DHC2-8) over the last 10 ka (constant water temperature), (2) there is <0.1‰ variation in contemporary calcite $\delta^{18}O$ at various sites throughout the cave (no gradients inside the submerged cave), and (3) U-series dating revealed that DHC2-8 precipitation rates of 0.1–0.8 μm a^{-1} are several orders of magnitude slower than laboratory-experiments, and *are thus less likely to induce kinetic fractionation*. It is important to note that Devil's Hole calcite precipitated in an open vertical shaft from ground water approximately 30 m below the water surface, and therefore solution–mineral precipitation kinetics are different from thin film degassing from splash drips atop a speleothem.

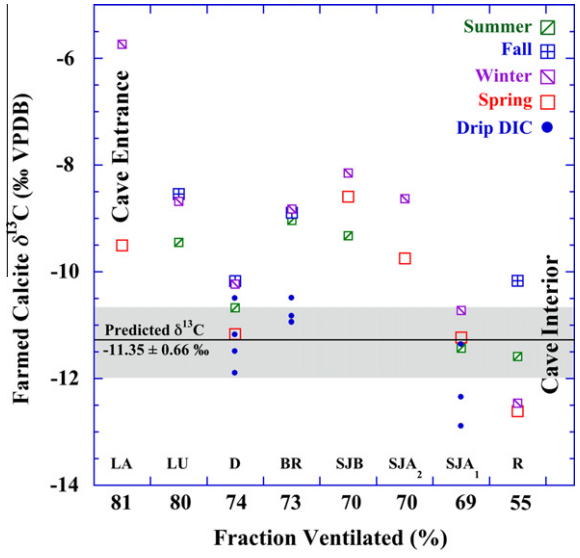

Fig. 8. Measured and predicted seasonal $\delta^{13}C$ of farmed calcite. *Y*-axis: predicted calcite $\delta^{13}C$ values (black line) based on 50:50 stoichiometric contributions of Oligocene limestone ($\delta^{13}C = -2‰$) and soil gas ($\delta^{13}C = -20.7‰$) to drip water DIC plotted with measured drip water DIC (filled blue circles) and farmed calcite average $\delta^{13}C$ (open squares) for each season. *X*-axis: fraction ventilated (%) at each farming location: LA (Larry), LU (Lucky), D (Duece), BR (Ballroom), SJB (Smith Jones Room B), SJA_2 (Smith Jones Room A_2), SJA_1 (Smith Jones Room A_1), and R (Richard). Fraction ventilated $[100 * (1 - f_{SG})]$ was calculated by isotopic mass balance of cave air CO_2 grab samples on 5/22/09 where f_{SG} is the fraction of soil gas in each sample, $\delta^{13}C_{Sample}[CO_2]_{Sample} = f_{Atm}\ \delta^{13}C_{Atm}\ [CO_2]_{Atm} + f_{SG}\ \delta^{13}C_{SG}\ [CO_2]_{SG}$ and $f_{Atm} + f_{SG} = 1$. Measured endmembers are given in Table EA.8. Shaded area indicates the observed ±0.66‰ (1σ) range in soil gas $\delta^{13}C$. During winter, spring, and summer Smith and Jones A1 and Richard calcite $\delta^{13}C$ values are consistent with predicted drip ^{13}C. During spring and summer Duece calcite is also consistent with predicted drip ^{13}C. All other sites exhibit a significant enrichment in ^{13}C suggesting either rapid CO_2 degassing (Hendy, 1971) or equilibrium precipitation with some percentage of cave air-derived DIC. In both cases, a shift toward higher calcite $\delta^{13}C$ values indicates ventilation effects on calcite isotopic composition.

Three basic factors control isotope fractionation during mineral–solution interaction: (1) forward reaction rate and kinetic fractionation factor (R_f and α_f); (2) the equilibrium fractionation factor (α_e); and (3) the backward (dissolution) reaction rate (R_b) defined as the difference between the net precipitation rate and the forward reaction rate ($R_p - R_f$) (DePaolo, 2011). Calcite will form close to oxygen isotopic equilibrium under the conditions of ($R_p/R_b \ll 1$), in other words the *net* precipitation rate is very slow with respect to the gross forward and backward reactions. At faster net precipitation rates, the forward kinetic fractionation factor will control the isotope system ($R_p/R_b \geqslant 1$). Calcite growth kinetics studies (e.g., Teng et al., 2000) have demonstrated that calcite growth rate is directly proportional to the extent of supersaturation ($\Omega > 1$), i.e. higher Ω results in faster R_f. Higher values of Ω also decrease the solubility of $CaCO_3$ (*s*), resulting in reduced gross dissolution or R_b. From this reasoning we suggest that calcite precipitated very slowly in a cave environment from natural drips at low Ω is likely closer to oxygen isotope equilibrium than lab-based experiments performed at high Ω. Additional rationale for this assessment will be explored in Section 5.1.

4.6. Predicted and measured calcite $\delta^{13}C$ – ventilation effects

Several studies have quantified the effects of ventilation, fast degassing and carbon isotope exchange in the calcite–water–soil gas system in natural systems (Spötl et al., 2005; Frisia et al., 2011; Lambert and Aharon, 2011), in laboratory settings (Wiedner et al., 2008; Polag et al., 2010), and from a theoretical perspective (Scholz et al., 2009; Mühlinghaus et al., 2009; Dreybrodt and Scholz, 2011). In order to constrain the extent of ventilation-driven disturbances in equilibrium precipitation, it is necessary to know or assume the following: (1) carbon source endmember isotopic compositions; and (2) extent of isotopic exchange between drip water and cave air CO_2. We follow Mühlinghaus et al. (2009), Scholz et al. (2009) and Frisia et al. (2011) in assuming little or no ^{13}C fractionation between dissolved HCO_3^- and $CaCO_3$ based on the negligible temperature dependence ($HCO_3^- \rightarrow CaCO_3\ \varepsilon_2{}^{13} = -0.03‰$ at 6.5 °C) as reported by Mook and de Vriess, 2000.

Stoichiometric contributions of bedrock and soil gas CO_2-derived DIC are an ideal starting point for prediction of drip water DIC. The predicted drip water DIC for soil gas CO_2 ($\delta^{13}C = -20.7 \pm 0.66‰$) combined with Oligocene limestone (assumed $\delta^{13}C = -2.0‰$) is $\delta^{13}C = -11.35‰$. As discussed in Section 4.3, three drip sites (Duece, Smith and Jones A, and Ballroom) were sampled once monthly for four months to determine TCO_2 and carbonate speciation. Drip water DIC at those sites was measured to be $\delta^{13}C = -11.5 \pm 1‰$ (1σ range) (Table EA.4), indicating that measured values are in good agreement with predicted $\delta^{13}C$ values and that stoichiometric carbon transport through the soil-epikarst system is an acceptable assumption, at least for winter time conditions.

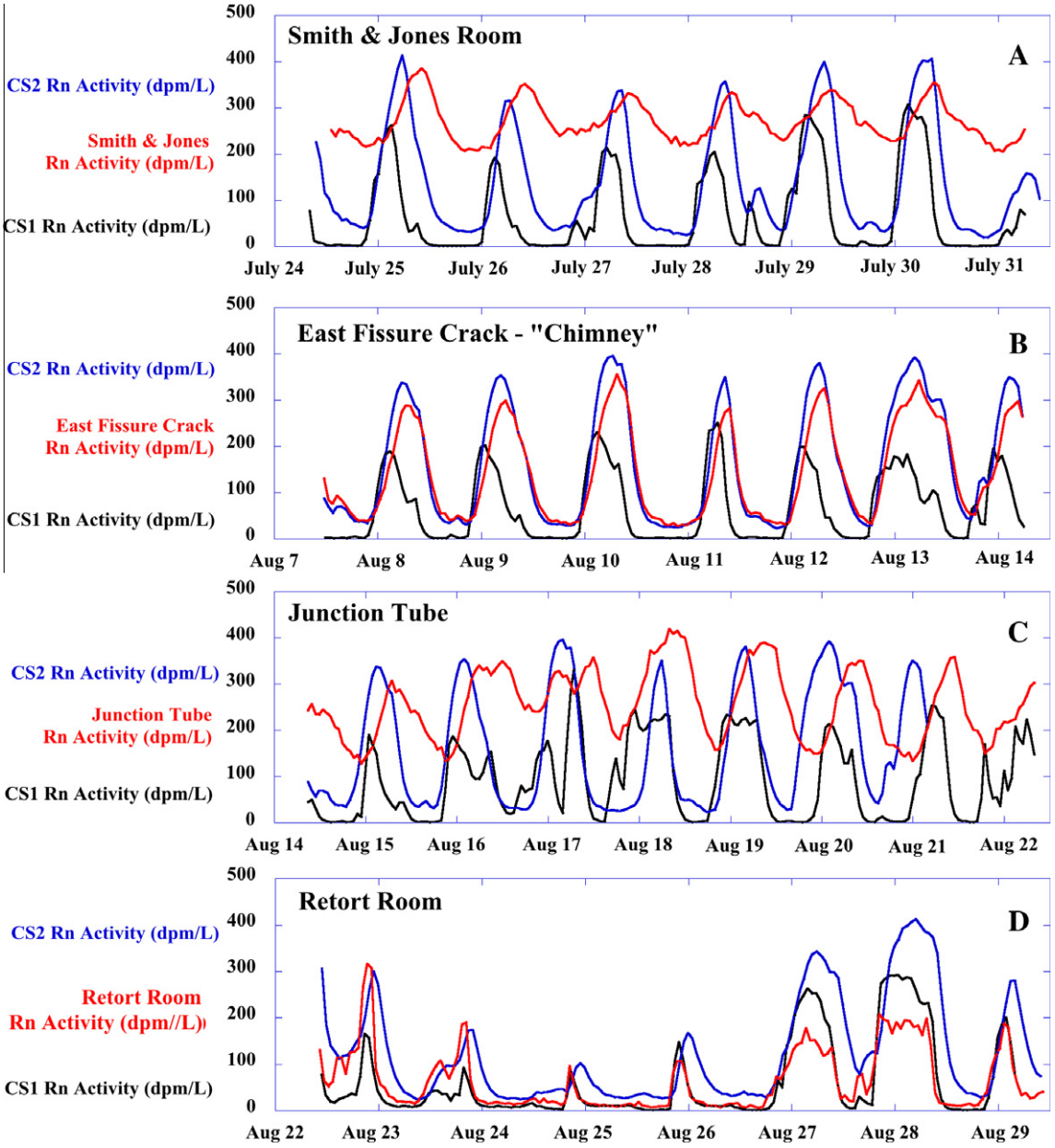

Fig. 9. Multiple room ^{222}Rn activities compared with Cave Station 1 (Entrance Room) and Cave Station 2 (Signature Room) for four different one week periods in July and August 2009 (see Fig. 1 for locations). The *x*-axis of each panel displays time in 24-hour intervals (days), with tick marks denoting mid-night. Cave Station 2 (CS2) radon activity is shown in blue. Cave Station 1 (CS1) activity is shown in black. Radon activity in each room is shown in red; (A) Smith and Jones Room; (B) East End of Fissure Crack; (C) Junction Tube; (D) Retort Room. Several locations inside Hollow Ridge such as Smith and Jones and the Junction Tube do not experience full ventilation in the down-drafting summer ventilation regime.

Most of the calcite plates display $\delta^{13}C$ values that are heavier than their respective drips (Fig. 8). Calcite grown at Ballroom, Smith and Jones B, Smith and Jones A2, as well as Lucky, and Larry (both near Entrance A – Fig. 1) exhibit a +1.5‰ to +2.7‰ enrichment in $\delta^{13}C$ during spring and summer (weak ventilation), and a +2.7‰ to +5.5‰ enrichment during winter and fall (strong ventilation regime). Larry and Lucky are closest to Entrance A, and show winter time enrichments of +5.5‰ over predicted values. Sites Duece and Smith and Jones A1 precipitate calcite $\delta^{13}C$ that are consistent with predicted values during spring and summer, and are enriched in ^{13}C by +0.7‰ to 1.0‰ during fall and winter, about half that of the other sites. Site Richard precipitates calcite consistent with predicted $\delta^{13}C$ values during summer, spring, and winter, but exhibit a +1.8‰ enrichment during fall.

4.7. Whole cave Hendy test relationships

Calcite grown at sites within the faster ventilation pathways of the cave (Larry, Lucky, Ballroom, Smith and Jones Site B, Smith and Jones Site A2) all have isotopic signatures

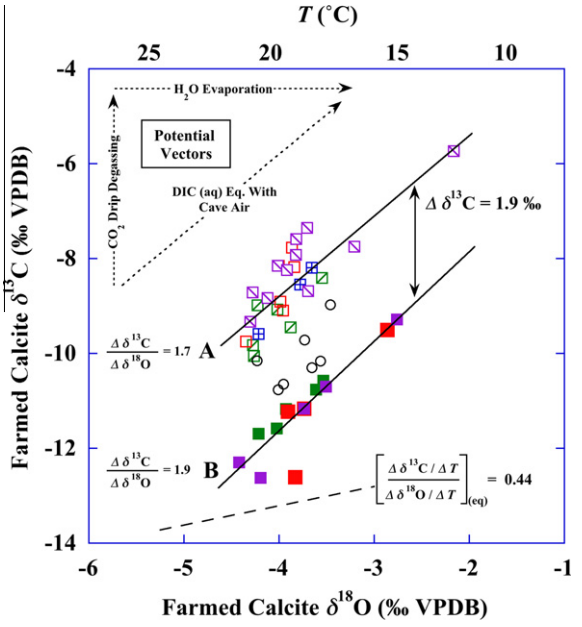

Fig. 10. Seasonal farmed calcite $\delta^{13}C$ vs. $\delta^{18}O$ (Hendy test). The top *x*-axis is estimated cave temperature (°C) at each location. Open symbols (summer: green squares; fall: blue squares: winter: purple squares; and spring: red squares) represent samples that precipitated in ventilation flow path, while closed shapes with the same color designations represent samples precipitated out of ventilation flow path. Open circles represent sites that experience intermediate ventilation and are not included in the linear regressions. Vertical dotted arrow represents the predicted geochemical vector for fast drip CO_2 degassing. Horizontal dotted arrow represents predicted vector for fast water evaporation. The diagonal dotted vector indicates equilibrium precipitation with a mixture of soil gas and limestone derived DIC ($\delta^{13}C \sim -11.35‰$) and cave air CO_2-derived DIC ($\delta^{13}C \sim -2‰$) over a range of *in situ* temperatures. The dashed black line with slope $\Delta\ \delta^{13}C/\Delta\ \delta^{18}O = 0.44$ indicates the predicted temperature dependent equilibrium slope as discussed in Section 4.7. Solid lines through each subset of data are linear best-fit lines. Line A: $\delta^{13}C = 1.7\ (\delta^{18}O) - 2.1‰$; Line B: $\delta^{13}C = 1.9\ (\delta^{18}O) - 4.0‰$. Farming sites on Line A (summer: Lucky, Ballroom, and Smith and Jones B; fall: Lucky, Ballroom, and Richard; winter: Larry, Lucky, Ballroom, Smith and Jones B, Smith and Jones A1 and A2; spring: Larry, Smith and Jones B, and Smith and Jones A2) experience ventilation-driven CO_2 degassing as indicated by a $+1.9 \pm 0.96‰$ (1σ) shift in $\delta^{13}C$ $CaCO_3$. Unlike $\delta^{13}C$, the 2.2‰ range in $\delta^{18}O$ is due to the 9.5 °C difference in growth temperatures.

1–5‰ more enriched in ^{13}C than predicted (Fig. 8). Calcite $\delta^{13}C$ is high near the entrances of the cave and becomes lower in the depths of the cave where ventilation is weakest. Radon measurements at several locations, including the Smith and Jones room near Site A, indicate that full ventilation is not achieved at all sites during the summer (Fig. 9). These results imply that ventilation affects calcite $\delta^{13}C$ along a spectrum between two mixing endmembers: (1) outside atmospheric air (low pCO_2, high $\delta^{13}C$) entering at the cave entrance drives rapid drip water CO_2 degassing, preferentially removing the light isotope ($^{12}CO_2$) and enriching the remaining HCO_3^- – $\delta^{13}C$ (aq) reservoir (and consequent calcite); and (2) the initial aqueous HCO_3^- in the drip water which is also a mixture of soil gas and ^{13}C enriched atmospheric air ($\delta^{13}CO_2 = -10‰$), the composition of which is dependent on seasonal and diurnal ventilation gradients as depicted in Figs. 3 and 4.

To test the effects of ventilation on farmed calcite $\delta^{13}C$ and $\delta^{18}O$, we constructed a modified "Hendy test" diagram of our farmed calcite ^{18}O vs. ^{13}C data (Fig. 10). Hendy (1971) predicted that rapid $^{12}CO_2$ degassing from drip waters would drive the carbon isotopic composition of calcite toward higher $\delta^{13}C$ values with no change in $\delta^{18}O$, provided that the degassing rate is slow enough to allow continuous ^{18}O equilibrium exchange with the water oxygen isotope reservoir. Alternatively, drip water degassing and rapid precipitation would drive both $\delta^{13}C$ and $\delta^{18}O$ toward higher values. The "Hendy test" is often employed along a growth layer in a stalagmite to establish if a speleothem was precipitated out of oxygen isotopic equilibrium with drip water, and assumes a "closed" carbon system.

In order to test this conceptual model, we first predict what the temperature-induced changes in $\delta^{18}O_{CaCO3}$ and $\delta^{13}C_{CaCO3}$ would be at isotopic equilibrium by calculating the temperature-dependent slope based on the results of Deines et al. (1974) and Kim and O'Neil (1997) (Eq. (4.5.4)):

$$[\Delta\delta^{13}C/\Delta T]/[\Delta\delta^{18}O/\Delta T] = -0.09‰ / -0.206‰ = 0.44 \quad (4.7.1)$$

This "slope of the slopes" is then the predicted change in $\delta^{13}C$ and $\delta^{18}O$ of calcite precipitated under equilibrium conditions from a homogeneous aquatic reservoir of fixed isotopic composition due only to changes in temperature. Note that slight differences in which temperature coefficients one chooses (which literature values) makes very little difference in this value. This slope is plotted on Fig. 10 near the bottom.

The Hendy test should then be judged against this equilibrium slope. It is important to make the distinction that the Hendy model is a Rayleigh fractionation model of calcite precipitated from an isolated and increasingly isotopically heavy solution, whereas we apply the concept not to one stalagmite growth layer but to an entire cave system in both time and space. Our farmed calcite was precipitated at many locations during different growth seasons throughout the cave, and the $\delta^{13}C/\delta^{18}O$ of each sample is controlled by (1) temperature of formation ($\delta^{18}O$), (2) the pCO_2 gradient between water and air driving drip water CO_2 degassing ($\delta^{13}C$), and (3) the equilibrated fraction of cave air-derived DIC in drip water ($\delta^{13}C$). Two groupings are observed in our farmed calcite (Fig. 10): (1) those precipitated in carbon equilibrium with drip water, and (2) those precipitated in a strongly ventilated flow path. The two groupings have very similar slopes ($\Delta\delta^{13}C/\Delta\delta^{18}O = 1.7$ and 1.9) which are steeper than predicted for temperature equilibration only (0.44). But those in the ventilated flow path are offset in $\delta^{13}C$ from those outside the flow path by $+1.9 \pm 0.6‰$ (1σ). Both groupings exhibit CO_2 ventilation effects as indicated by a slope steeper than predicted (~1.8 versus 0.44 – Eq. (4.7.1)). But unlike $\delta^{13}C$, the 2.2‰ range in $\delta^{18}O$ is a result of the 9.5 °C temperature difference between farming

sites as indicated by the top x-axis in Fig. 10 ($\Delta\delta^{18}O_{CaCO3}/\Delta T \sim -0.23‰/°C$). We therefore assume, but can not prove, that the calcite $\delta^{18}O$ increase is due entirely to temperature-induced fractionation effects and not due to enhanced evaporation along the ventilation pathway (for example, see Day and Henderson, 2011). Relative humidity measured at CS1 and CS2 always fell between 97% and 100%, suggesting minimal evaporation effects. More work is needed to document this effect.

The +1.9‰ offset in the $\delta^{13}C$ gradients (Fig. 10) represents a difference between sites that are only slightly ventilated and those that are vigorously ventilated. Since the oxygen isotopic composition is (in this case) a ventilation-independent variable, the slope of each line is set by the air-water pCO_2 gradient along the flow path. The observed shift in $\delta^{13}C$ is not likely due to differences in degassing rates since there is no accompanying change in the $\Delta\delta^{13}C/\Delta\delta^{18}O$ slope between groupings. Instead, we argue that the shift is due to equilibrium precipitation with a mixture of soil gas ($\delta^{13}C = -20.7‰$) and limestone ($\delta^{13}C \sim -2‰$) derived DIC and cave air CO_2-derived DIC ($\delta^{13}C$ is variable – see Fig. 3).

Air grab transects throughout Hollow Ridge Cave at different times of year reveal that significant portions of the cave are ventilated as a function of depth into the cave interior. Summer cave-air CO_2 in the stream of the ventilation flow path can be 75% atmospheric air, and during periods of vigorous winter ventilation, cave air samples are often 100% forest canopy air (−10‰ at 450 ppmv – Fig. 4F). Using predicted ranges in drip water $\delta^{13}C_{DIC}$, measured calcite $\delta^{13}C$, and measured ranges in cave air $\delta^{13}C$, we performed a simple mass balance to determine the fraction of DIC equilibration with cave air necessary to produce the observed offsets in calcite $\delta^{13}C$:

$$\delta^{13}C_{CaCO3} = f_{DIC(SG)} \times \delta^{13}C_{DIC(SG)} + f_{DIC(Cave\ Air)} \times \delta^{13}C_{DIC(Cave\ Air)} \quad (4.7.2)$$

$$1 = f_{DIC(SG)} + f_{DIC(Cave\ Air)} \quad (4.7.3)$$

where $f_{DIC\ (SG)}$ and $f_{DIC\ (Cave\ Air)}$ are the respective fractions of soil gas and cave air-derived DIC, and $\delta^{13}C_{DIC\ (SG)}$ and $\delta^{13}C_{DIC\ (Cave\ Air)}$ are the predicted isotopic compositions of soil gas and cave air-derived DIC. We assume no fractionation between DIC-$\delta^{13}C$ and $CaCO_3$–$\delta^{13}C$. Isotope mass balance for Hollow Ridge Cave calcite indicates that the entire range of variation in $\delta^{13}C_{CaCO3}$ can be accounted for with a 30–60% cave air contribution to drip water DIC (consistent with the mixing in Fig. 3), while calculations of Frisia et al. (2011) demonstrate a cave air-CO_2 contribution to drip water DIC on the order of 25–30%.

The question often arises whether the CO_2 released from direct calcite precipitation is a significant proportion of the CO_2 inside a cave. We again take a mass balance approach to determine the relative contribution of degassed CO_2 as a control on calcite isotopic composition. We estimate the proportion of degassed CO_2 in cave air by taking an average calcite deposition rate of 121 μmol m^{-2} h^{-1} (Table EA.3), an estimated cave area of 3324 m^2 (approximately 10% of which is actively precipitating calcite), and the stoichiometric weight fraction of CO_2 in calcite (44 g CO_2/100 g $CaCO_3$) as follows:

$$\frac{121\ \mu mol}{m^2\ h} \times \frac{3324\ m^2}{10} \times \frac{44.01\ g\ CO_2}{100.09\ g\ CaCO_3} = 17.68\ mmol\ CO_2\ h^{-1} \quad (4.7.4)$$

Compared to average summer and winter CO_2 fluxes from Hollow Ridge Cave exhaled to the atmosphere as calculated by Kowalczk and Froelich (2010) of 5 mol h^{-1} (summer), and 0.5 mol h^{-1} (winter), the calcite-released CO_2 contribution to the total CO_2 reservoir (cave air and drip water) is approximately 0.35–3.5% mol fraction. Thus calcite $\delta^{13}C$ is not likely to be significantly impacted by re-equilibration with calcite-derived CO_2.

Although these results need to be repeated in other cave systems, we suggest that since all caves that precipitate calcite speleothems must breathe to remove CO_2 and to oversaturate drips with respect to calcite (Kowalczk and Froelich, 2010), then all speleothems are susceptible to these ventilation effects on $\delta^{13}C$. Whether these ventilation effects may also affect $\delta^{18}O$ due to evaporation along airways is yet to be established.

5. DISCUSSION

5.1. Approaching oxygen isotope equilibrium precipitation

Low-temperature (LT) laboratory calcite precipitation experiments are usually performed by dissolving reagent grade $CaCO_3$ in CO_2 charged distilled water, or by adding metal salts ($CaCl_2$, $MgCl_2$, etc.) to a $NaHCO_3$ solution (Table EA.6). Calcium carbonate precipitation is then driven by bubbling molecular nitrogen (N_2) through the solution to strip dissolved $CO_{2(aq)}$ out of solution. Such experiments give broadly reproducible results, and are generally in accord with theoretical predictions based on statistical-mechanical calculations of reduced partition functions such as those carried out by Urey (1947), Chacko et al. (1991), Dove et al. (1992), Watson (2004), Horita and Clayton (2007) and most recently Chacko and Deines (2008). However, it is virtually impossible to prove in laboratory or cave settings that calcium carbonate precipitated at LT from aqueous solution is in oxygen isotopic equilibrium.

Precipitation processes in LT lab experiments are most likely to approach oxygen isotopic equilibrium when performed at extremely slow rates of precipitation (Horita and Clayton, 2007; DePaolo, 2011). Kim and O'Neil (1997) performed inorganic precipitation experiments at three temperatures (10, 25 and 40 °C) with three solutions containing varying calcium concentrations; $[Ca^{2+}] = 5$, 15, and 25 mmol L^{-1}. They argued that the 5 mmol L^{-1} starting solution was most like natural waters and was most likely in isotopic equilibrium. Their 15 and 25 mmol L^{-1} solutions showed much larger fractionation at 10 and 25 °C and were thus thought to have precipitated calcite out of equilibrium. Moreover, increased initial oversaturation (precipitation rate) resulted in an increase in the apparent temperature dependence (steeper slope of 1000 ln α vs. $10^3\ T^{-1}$) of oxygen isotopic fractionation. Because the slope

of the Kim and O'Neil (1997) 5 mmol L^{-1} experimental line closely agreed with earlier studies that included extrapolated lines from high temperature 'equilibrium' experiments and biogenic calcite (O'Neil et al., 1969; Grossman and Ku, 1986; Patterson et al., 1993), and because more dilute solutions reportedly gave fractionation factors that approached a limiting value, the 5 mM experiment was accepted as most likely to represent equilibrium precipitation. However, Kim and O'Neil (1997) admitted that these were "*only plausibility arguments as attainment of isotopic equilibrium can not be proved*." Furthermore, they stated that future experiments involving extremely dilute solutions would be performed, ostensibly to discover the lower limit. Later experiments (Kim et al., 2007) served to lower the *y*-intercept to −32.17 as a result of adopting an acid fractionation factor ($\alpha_{CO2(ACID)–Calcite}$) of 1.01030‰ instead of the previously calculated 1.01055‰. However the lower limits of the temperature dependence (slope of 1000 ln α vs. $10^3\ T^{-1}$) were not investigated.

Kim and O'Neil (1997) stated that "*we judge the smallest fractionation factors obtained to be the best representation of equilibrium fractionation factors. This judgment may seem counterintuitive to those who would expect kinetically-controlled, non-equilibrium fractionations to be too small.*" In contrast, Coplen (2007) noted that "*Kinetic considerations may suggest preferential incorporation of the isotopically light species (e.g., CO_3^{2-}) during rapid precipitation.*" In other words, during rapid precipitation there should be less discrimination against ^{16}O, which would result in isotopically lighter calcite and lower fractionation factors. Values of $\delta^{18}O$ in inorganic carbonates precipitated in laboratory settings have been reported to be independent of growth rate (Tarutani et al., 1969; Kim and O'Neil, 1997; Jimenez-Lopez et al., 2001). However, our calculations (Table EA.7) show that the initial starting concentrations of Kim and O'Neil (1997) result in solutions that are one to three orders of magnitude more supersaturated with respect to calcite than those measured in HRC and Devil's Hole, possibly driving the kinetic effects cited by the authors. As previously discussed, higher Ω drives increased forward reaction (R_f) and decreased dissolution (R_b), thus kinetic fractionation becomes the dominant control of calcite $\delta^{18}O$. Therefore carbonates grown under conditions of $\Omega \gg 1$ should not be expected *a priori* to precipitate in oxygen isotopic equilibrium with the parent solution (DePaolo, 2011).

Another major difference between laboratory and cave experiments is that nitrogen is bubbled through lab solutions to strip CO_2 (aq) out of solution to drive $CaCO_3$ precipitation. Active nitrogen (N_2) bubble degassing of bulk fluids is very different from passive CO_2 degassing through a thin film from a liquid droplet or rivulet. In cave air the minimum pCO_2 is set by the local ventilation regime (Figs. 2 and 3), and a completely ventilated cave has a minimum pCO_2 condition of atmospheric air at approximately 390 ppmv. During drip water degassing cave air CO_2 diffuses into the drip while CO_2 (aq) diffuses out of the drip, with a net CO_2 loss from the drip, analogous to the surface ocean (Zeebe et al., 1999). During this process, water CO_2 slowly reaches isotopic equilibrium with cave air CO_2 on the order of minutes (Dreybrodt and Scholz, 2011), and aqueous carbonate species, almost all bicarbonate ions, contain oxygen that is near or at equilibrium with drip water. In contrast, bubbling N_2 in the laboratory experiment essentially exposes the solution to a 0 ppmv CO_2 atmosphere which strips $CO_{2(aq)}$ out of solution much more quickly. Such CO_2 transport is essentially a one-way process with no avenue of re-equilibration. It is possible that N_2 bubbling causes large kinetic fractionation between carbonate species, which may involve the preferential deprotonation of isotopically light HCO_3^- and the incorporation of the light CO_3^{2-} isotopologues as proposed by Kim et al. (2006).

Dietzel et al. (2009) attempted to circumvent N_2 bubbling by introducing a high pCO_2 $NaHCO_3$ solution to a low pCO_2 $CaCl_2$ solution through a semi-permeable polyethylene membrane (Dietzel and Usdowski, 1996). At constant pH, Dietzel et al. (2009) and Kim et al. (2006) both demonstrated a systematic *increase* in $\alpha_{CaCO3–H2O}$ with increasing experimental duration (slower precipitation). However, based on our interpretation of the disequilibrium isotope offset, calcite precipitated by Dietzel et al. (2009) is the farthest from equilibrium, for reasons that are not understood.

Coplen (2007) and Dietzel et al. (2009) provide compelling arguments that laboratory inorganic calcite precipitation experiments *underestimate* equilibrium fractionation factors between water and calcite. A linear best-fit line through data from a large number of modern cave studies (Fig. 7) suggests that the equilibrium fractionation of calcite in a "natural cave laboratory" is:

$$1000 \ln \alpha = [16.1 \pm 0.65]\ (10^3\ T^{-1}) - [24.6 \pm 2.2]$$
$$R^2 = 0.94\ (98\%\ \text{C.I.}) \qquad (5.1.1)$$

$$\Delta\delta^{18}O\ CaCO_3/\Delta T = -0.177‰/^{\circ}C \qquad (5.1.2)$$

This "cave calcite" line describes samples that were precipitated at many different latitudes, altitudes, and temperatures. In Fig. 7 the "cave" line intersects the O'Neil et al. (1969) line at $T = 0$ °C, which suggests a systematic offset between the "cave" line and laboratory predictions at higher temperatures. Although we cannot fully explain the systematic offset, it is clear that additional empirical calibrations of this nature are essential to the interpretation of paleoclimate and paleotemperature data from caves.

5.2. Ventilation

We have demonstrated that ventilation in a shallow cave can have significant impacts on calcite $\delta^{13}C$, and that seasonal ventilation regimes control the rate and timing of calcite precipitation. In general, atmospheric CO_2 mixes with soil gas inside the cave, and calcite precipitates in equilibrium with a ^{13}C-enriched DIC reservoir as a function of distance along the ventilated flow path. At present micro-mill sampling resolution (50–500 μm) ventilation-induced seasonal variations in calcite $\delta^{13}C$ are likely overprinted by climate-driven long-term changes in cave air CO_2. However, significant calcite $\delta^{13}C$ shifts could arise

from long-term changes in ventilation without concomitant changes in either vegetation or atmospheric CO_2. Modern HRC calcite exhibits a $-7‰$ $\delta^{13}C$ gradient along the ventilation pathway from cave entrance to interior during the winter. Entrance collapse would slow ventilation, and calcite near the entrance would take on the isotopic signature of DIC, thus eliminating the gradient. Conversely, the introduction of a new ventilation pathway to the interior of the cave may drive calcite to less ^{13}C depleted values. Such an excursion might be mistakenly interpreted as a rapid increase in the ratio of C4/C3 vegetation overlying the cave. Thus, it may be useful to begin thinking of rapid changes in calcite $\delta^{13}C$ as possible perturbations in the dominant paleo-ventilation regime, as cave openings come and go with the evolving karst hydrology.

6. CONCLUSIONS

Calcite farming in continuously monitored Hollow Ridge Cave (HRC) has revealed for the first time a direct connection between calcite growth rates, seasonal calcite $\delta^{13}C$ and ventilation-driven pCO_2 gradients inside a cave. Calcite $\delta^{13}C$ decreases along the ventilation pathway suggesting that calcite $\delta^{13}C$ is a potential proxy not only for overlying vegetation or atmospheric CO_2, but also for cave air ventilation. Indeed, seasonal ventilation-driven variations in speleothem $\delta^{13}C$ would not likely be obvious without high-resolution calibrations in both time and space. As in other caves, summer-time air stagnation inside HRC leads to high cave air pCO_2 that reduces drip water CO_2 degassing and thus lowers calcite precipitation rates. We predict that this reduction would result in seasonal aliasing of the calcite climate signal toward winter-time climates. Since all caves with actively growing formations must experience ventilation to remove cave air CO_2 that drive the precipitation reaction, these inferences are generally applicable to all caves that breathe.

Modern *in situ* calibration of calcite $\delta^{18}O$-temperature fractionation factors in HRC farmed calcite has demonstrated that inorganic calcite precipitated very slowly from slightly supersaturated drip solutions is more enriched in ^{18}O ($+0.82 \pm 0.24‰$) than predicted from laboratory-based inorganic calcite precipitation experiments. Based on our calibrations and data from other cave investigations, we propose a new empirical isotope-temperature fractionation relationship for inorganic cave calcite:

$$1000 \ln \alpha = 16.1\left(10^3\ T^{-1}\right) - 24.6$$

This equation defines a temperature-dependent oxygen isotope fractionation of approximately $\Delta\delta^{18}O\ CaCO_3/\Delta T = -0.177‰/°C$. We suggest that laboratory-based inorganic calcite precipitation experiments suffer from poorly understood kinetic isotope effects that drive the perceived 'classic' temperature dependence higher, to $-0.206‰/°C$.

Although water–calcite oxygen isotope equilibrium is not likely to be achieved either in caves or in laboratories, we suggest that natural cave calcite is precipitated more slowly and is likely closer to equilibrium than laboratory experiments. Modified "Hendy tests" from *in situ* farmed HRC calcite produce $\Delta\delta^{13}C/\Delta\delta^{18}O$ relationships with slopes ($\sim$1.8) that are higher than that predicted based on equilibrium temperature alone ($\sim$0.44). Similar relationships have been reported from numerous cave studies, further suggesting the possibility that nature, while seemingly reproducible, may not precipitate calcite in isotopic equilibrium. However, we demonstrate that this slope and concomitant $\delta^{13}C$ offsets are the result of small temperature differences in $\Delta\delta^{18}O$ and large cave air ventilation effects in $\Delta\delta^{13}C$. Thus the application of a whole-cave "Hendy test", commonly used to discriminate "equilibrium" calcite precipitation in speleothem growth layers, may in fact be an extremely useful ventilation proxy in the absence of traditional proxy measurements such as CO_2 or ^{222}Rn.

ACKNOWLEDGMENTS

This research is conducted in conjunction with the Southeastern Cave Conservancy Inc. (SCCi), PO Box 71857, Chattanooga, TN 37407-0857, Chairman: B. Krebs, with financial support from D. Baker, Plum Creek Timber, Seattle, WA. We thank A. Mosler, HRC SCCi cave steward for allowing unrestricted access to HRC and for generous field support. We thank A. Kowalczk for creating and deploying the cave monitoring equipment, and B. Kilgore for continuous field support, sample collection, and anion analyses, and J. Chanton, S. Misra, Y. Xu, C. Langford, and J. Corbett for analytical assistance. We thank D. Nof for his input on ventilation dynamics and the cartoon of cave ventilation. We thank M. Humayun, W. Burnett, and T. Coplen for internal reviews of earlier drafts. We thank Mira Bar-Matthews for meticulous editorial handling and three anonymous reviewers for their thoughtful criticism that helped focus and refine this manuscript. This work was funded by Florida State University Francis Eppes Foundation and NSF grant #AGS-1032403 to P.N.F., and by an FSU-Oceanography teaching assistantship to D.T.

APPENDICES A AND B. SUPPLEMENTARY DATA

Supplementary data associated with this article can be found, in the online version, at doi:10.1016/j.gca.2011.06.005.

REFERENCES

Baker A., Smart P., Edwards R. and Richards D. (1993) Annual growth banding in a cave stalagmite. *Nature* **364**, 518–520.

Baker A., Smith C., Jex C., Fairchild I., Genty D. and Fuller L. (2008) Annually laminated speleothems: a review. *Int. J. Speleol.* **37**, 193–206.

Baldini J., McDermott F. and Fairchild I. (2006a) Spatial variability in cave drip water hydrochemistry: implications for stalagmite paleoclimate records. *Chem. Geol.* **235**, 390–404.

Baldini J. U. L., Baldini L. M., McDermott F. and Clipson N. (2006b) Carbon dioxide sources, sinks, and spatial variability in shallow temperate zone caves: evidence from Ballynamintra Cave, Ireland. *J. Cave Karst Stud.* **68**, 4–11.

Baldini J., McDermott F., Hoffmann D., Richards D. and Clipson N. (2008) Very high-frequency and seasonal cave atmosphere PCO_2 variability: implications for stalagmite growth and

oxygen isotope-based paleoclimate records. *Earth Planet. Sci. Lett.* **272**, 118–129.

Banner J. L., Guilfoyle A., James E., Stern L. and Musgrove M. (2007) Seasonal variations in modern speleothem calcite growth in Central Texas, USA. *J. Sed. Res.* **77**, 615–622.

Bar-Matthews M., Ayalon A. and Kaufman A. (1997) Late Quaternary paleoclimate in the eastern Mediterranean region from stable isotope analysis of speleothems at Soreq Cave, Israel. *Quatern. Res.* **47**, 155–168.

Bar-Matthews M., Ayalon A., Gilmour M., Mathews A. and Hawkesworth C. J. (2003) Sea–land oxygen isotopic relationships from planktonic foraminifera and speleothems in the Eastern Mediterranean region and their implication for paleorainfall during interglacial intervals. *Geochim. Cosmochim. Acta* **67**, 3181–3199.

Baskaran M. and Krishnamurthy R. V. (1993) Speleothems as proxy for the carbon isotope composition of atmospheric CO_2. *Geophys. Res. Lett.* **20**, 2905–2908.

Boch R. (2008) Stalagmites from Katerloch Cave, Austria: growth dynamics and high-resolution records of climate change. Ph. D. dissertation, Leopold-Franzens University of Innsbruck, Austria. Available from: <http://www.uibk.ac.at/geologie/staff/boch_en.html>.

Boch R., Spötl C. and Kramers J. (2009) High-resolution isotope records of early Holocene rapid climate change from two coeval stalagmites of Katerloch Cave, Austria. *Quatern. Sci. Rev.* **28**, 2527–2538.

Bourges F., Genthon P., Mangini A. and D'Hulst D. (2006) Microclimates of L'Aven D'Orgnac and other French limestone caves (Chauvet, Esparros, Marsoulas). *Int. J. Climatol.* **26**, 1651–1670.

Boyer P. R. (1975) Hollow Ridge Cave. Southeastern Karst Survey General Report: 2.

Brook G. A., Burney D. A. and Cowart B. J. (1990) Desert paleoenvironmental data from cave speleothems with examples from the Chihuahuan, Somali-Chalbi, and Kalhari deserts. *Paleogeogr. Paleoclimatol. Paleoecol.* **76**, 311–329.

Burns S. J., Fleitmann D., Mudelsee M., Neff U., Matter A. and Mangini A. (2002) A 780-year annually resolved record of Indian Ocean monsoon precipitation from a speleothem from south Oman. *J. Geophys. Res.* **107**(D20), 4434. doi:10.1029/2001JD001281.

Chacko T., Mayeda T. K., Clayton R. N. and Goldsmith J. R. (1991) Oxygen and carbon isotope fractionations between CO_2 and calcite. *Geochim. Cosmochim. Acta* **55**, 2867–2882.

Chacko T. and Deines P. (2008) Theoretical calculation of oxygen isotope fractionation factors in carbonate systems. *Geochim. Cosmochim. Acta* **72**, 3642–3660.

Cheng H., Edwards R., Wang Y., Kong X., Ming Y., Kelly M., Wang X., Gallup C. and Liu W. (2006) A penultimate glacial monsoon record from Hulu Cave and two-phase glacial terminations. *Geology* **34**, 217–220.

Cheng H., Edwards R. L., Broecker W. S., Denton G. H., Kong X., Wang Y., Zhang R. and Wang X. (2009) Ice age terminations. *Science* **326**, 248–252.

Clemens S. C., Prell W. L. and Sun, Y. (2010) Orbital-scale timing and mechanisms driving Late Pleistocene Indo-Asian summer monsoons: reinterpreting cave speleothem $\delta^{18}O$. *Paleoceanography* 25, PA4207, 19pp., doi:10.1029/2010PA001926.

Cobb K. M., Adkins J. F., Partin J. W. and Clark B. (2007) Regional-scale climate influences on temporal variations of rainwater and cave dripwater oxygen isotopes in northern Borneo. *Earth Planet. Sci. Lett.* **263**, 207–220.

Coplen T. B. (1996) New guidelines for the reporting of stable hydrogen, carbon, and oxygen isotope-ratio data. *Geochim. Cosmochim. Acta* **60**, 3359–3360.

Coplen T. B., Brand W. A., Gehre M., Groning M., Meijer J. A. J., Toman B. and Verkouteren R. M. (2006) New guidelines for $\delta^{13}C$ measurements. *Anal. Chem.* **78**, 2439–2441.

Coplen T. B. (2007) Calibration of the calcite–water oxygen-isotope geothermometer at Devils Hole, Nevada, a natural laboratory. *Geochim. Cosmochim. Acta* **71**, 3948–3957.

Cosford J., Qing H., Mattey D., Eglington B. and Zhang M. (2009) Climatic and local effects on stalagmite $\delta^{13}C$ values at Lianhua Cave, China. *Palaeogeogr. Palaeoclimatol. Palaeoecol.* **280**, 235–244.

Craig H. (1961) Isotopic variations in meteoric waters. *Science* **133**, 1702–1703.

Cruz F., Burns S., Karmann I., Sharp W., Vuille M., Cardoso A., Ferrari J., Silva Dias P. and Viana O. (2005a) Insolation-driven changes in atmospheric circulation over the past 116,000 years in subtropical Brazil. *Nature* **434**, 63–66.

Cruz F., Karmann I., Viana O., Burns S., Ferrari J., Vuille M., Sial A. and Moreira M. (2005b) Stable isotope study of cave percolation waters in subtropical Brazil: implications for paleoclimate inferences from speleothems. *Chem. Geol.* **220**, 245–262.

Cruz F., Burns S., Jercinovic M., Karmann I., Sharp W. and Vuille M. (2007) Evidence of rainfall variations in Southern Brazil from trace element ratios (Mg/Ca and Sr/Ca) in a Late Pliestocene stalagmite. *Geochim. Cosmochim. Acta* **71**, 2250–2263.

Dansgaard W. (1964) Stable isotopes in precipitation. *Tellus* **16**, 436–468.

Day C. and Henderson G. (2011) Oxygen isotopes in calcite grown under cave-analogue conditions. *Geochim. Cosmochim. Acta.* **75**, 3956–3972.

Dayem K. E., Molnar P., Battisti D. S. and Roe G. H. (2010) Lessons learned from oxygen isotopes in modern precipitation applied to interpretation of speleothem records of paleoclimate from eastern Asia. *Earth Planet. Sci. Lett.* **295**, 219–230.

Deines P., Langmuir D. and Harmon R. S. (1974) Stable carbon isotope ratios and the existence of a gas phase in the evolution of carbonate ground waters. *Geochim. Cosmochim. Acta*, 1147–1164.

Dennis P. F., Rowe P. J. and Atkinson T. C. (2001) The recovery and isotopic measurement of water from fluid inclusions in speleothems. *Geochim. Cosmochim. Acta* **65**, 871–884.

Denniston R. F., DuPree M., Dorale J. A., Asmerom Y., Polyak V. J. and Carpenter S. J. (2007) Episodes of late Holocene aridity recorded by stalagmites from Devil's Icebox Cave, central Missouri, USA. *Quatern. Res.* **68**, 45–52.

DePaolo D. (2011) Surface kinetic model for isotopic and trace element fractionation during precipitation of calcite from aqueous solutions. *Geochim. Cosmochim. Acta* **75**, 1039–1056.

Desmarchelier J. M., Goede A., Ayliffe L. K., McCulloch M. T. and Moriarty K. (2000) Stable isotope record and its paleoenvironmental interpretation for a late Middle Pleistocene speleothem from Victoria Fossil Cave, Naracoorte, South Australia. *Quatern. Sci. Rev.* **19**, 763–774.

De Yoreo J., Zepeda-Ruiz L., Friddle R., Qiu S., Wasylenki L., Chernov A., Gilmer G. and Dove P. (2009) Rethinking classical crystal growth models through molecular scale insights: consequences of kink-limited kinetics. *Cryst. Growth Des.* **9**, 5135–5144.

Dietzel M. and Usdowski E. (1996) Coprecipitation of Ni^{2+}, Co^{2+}, and Mn^{2+} with galena and covellite, and of Sr^{2+} with calcite during crystallization via diffusion of H_2S and CO_2 through polyethylene at 20 °C: power law and Nernst law control of trace element partitioning. *Chem. Geol.* **131**, 55–65.

Dietzel M., Tang J., Leis A. and Kohler S. J. (2009) Oxygen isotopic fractionation during inorganic calcite precipitation – effects of temperature, precipitation rate and pH. *Chem. Geol.* **268**, 107–115.

Dorale J. A., Gonzalez L. A., Reagan M. K., Pickett D. A., Murrell M. T. and Baker R. G. (1992) A high-resolution record of Holocene climate change in speleothem calcite from Cold Water Cave, northeast Iowa. *Science* **258**.

Dove M. T., Winkler B. L. M., Harris M. J. and Slaje E. K. H. (1992) A new interatomic potential model for calcite: applications to lattice dynamics studies, phase transition, and isotope fractionation. *Am. Mineral.* **77**, 244–250.

Dreybrodt W. and Scholz D. (2011) Climatic dependence of stable carbon and oxygen isotope signals recorded in speleothems: from soil water to speleothem calcite. *Geochim. Cosmochim. Acta* **75**, 734–752.

Dykoski C., Edwards R., Cheng H., Yuan D., Cai Y., Zhang M., Lin Y., Qing J., An Z. and Revenaugh J. (2005) A high-resolution, absolute-dated Holocene and deglacial Asian monsoon record from Dongge Cave, China. *Earth Planet. Sci. Lett.* **233**, 71–86.

Ehleringer J. R., Cerling T. E. and Helliker B. R. (1997) C4 photosynthesis, atmospheric CO_2, and climate. *Oecologia* **112**, 285–299.

Epstein S., Buchsbaum R., Lowenstam H. and Urey H. C. (1951) Carbonate-water isotopic temperature scale. *Bull. Geol. Soc. Am.* **62**, 417–426.

Epstein S., Buchsbaum R., Lowenstam H. and Urey H. C. (1953) Revised carbonate-water isotopic temperature scale. *Bull. Geol. Soc. Am.* **64**, 1315–1326.

Fleitmann D., Burns S. J., Mudelsee M., Neff U., Kramers J., Mangini A. and Matter A. (2003a) Holocene forcing of the Indian monsoon recorded in a stalagmite from southern Oman. *Science* **300**, 1737–1739.

Fleitmann D., Burns S. J., Neff U., Mangini A. and Matter A. (2003b) Changing moisture sources over the last 330,000 years in Northern Oman from fluid-inclusion evidence in speleothems. *Quatern. Res.* **60**, 223–232.

Friedman I. and O'Neil J. R. (1977) Compilation of stable isotope fractionation factors of geochemical interest. *Geolog. Surv. Prof. Paper 440-KK*, pp. 117.

Frisia S., Borsato A., Fairchild I. and McDermott F. (2000) Calcite fabrics, growth mechanisms, and environments of formation in speleothems from the Italian Alps and Southwestern Ireland. *J. Sed. Res.* **70**, 1183–1196.

Frisia S., Fairchild I., Fohlmeister J., Miorandi R., Spötl C. and Borsato A. (2011) Carbon mass-balance modelling and carbon isotope exchange processes in dynamic caves. *Geochim. Cosmochim. Acta* **75**, 380–400.

Gascoyne M., Schwarcz H. P. and Ford D. C. (1980) A paleotemperature record for the mid-Wisconsin in Vancouver Island. *Nature* **285**, 474–476.

Gascoyne M. (1983) Trace-element partition coefficients in the calcite–water system and their paleoclimatic significance in cave studies. *J. Hydrol.* **61**, 213–222.

Genty D., Blamart D., Ouahdi R., Gilmour M., Baker A., Jouzel J. and Van-Exters S. (2003) Precise dating of Dansgaard-Oeschger climate oscillations in western Europe from stalagmite data. *Nature* **421**, 833–837.

Genty D. (2008) Paleoclimate research in Villars Cave (Dordogne, SW-France). *Int. J. Speleol.* **37**, 173–191.

Griffiths M. L., Drysdale R. N., Vonhof H. B., Cagan M. K., Zhao J., Ayliffe L. K., Hantoro W. S., Hellstrom J. C., Cartwright I., Frisia S. and Suwargadi B. W. (2010) Younger Dryas-Holocene temperature and rainfall history of southern Indonesia from $\delta^{18}O$ in speleothem calcite and fluid inclusions. *Earth Planet. Sci. Lett.* **295**, 30–36.

Grimm E., Jacobson G., Watts W., Hansen B. and Maasch K. (1993) A 50,000-year record of climate oscillations from Florida and its temporal correlation with the Heinrich events. *Science* **261**, 198–200.

Grimm E., Watts W., Jacobson G., Hansen B., Almquist H. and Dieffenbacher-Krall A. (2006) Evidence for warm wet Heinrich events in Florida. *Quatern. Sci. Rev.* **25**, 2197–2211.

Grossman E. L. and Ku T. (1986) Oxygen and carbon isotope fractionation in biogenic aragonite: temperature effects. *Chem. Geol.* **59**, 59–74.

Guilfoyle A. (2006) Temporal and spatial controls on cave water and speleothem calcite isotopic and elemental chemistry, central Texas. Master's thesis, University of Texas at Austin, Department of Geological Sciences, pp. 357.

Harmon R. S., Schwarcz H. P. and O'Neil J. R. (1979) D/H ratios in speleothem fluid inclusions: a guide to variations in the isotopic composition of meteoric precipitation?. *Earth Planet. Sci. Lett.* **42** 254–266.

Hendy C. (1971) The isotopic geochemistry of speleothems. *Geochim. Cosmochim. Acta* **35**, 801–824.

Holland H., Kirsipu T., Huebner J. and Oxburgh U. (1964) On some aspects of the chemical evolution of cave waters. *J. Geol.* **72**, 36–67.

Horita J. and Clayton R. N. (2007) Comment on the studies of oxygen isotope fractionation between calcium carbonates and water at low temperatures by Zhou and Zheng (2003, 2005). *Geochim. Cosmochim. Acta* **71**, 3131–3135.

Hou J. Z., Tan M., Cheng H. and Liu T. S. (2003) Stable isotope records of plant cover change and monsoon variation in the past 2200 years: evidence from laminated stalagmites in Beijing, China. *Boreas* **32**.

Jimenez-Lopez C., Caballero E., Huertas F. J. and Romanek C. S. (2001) Chemical, mineralogical and isotope behavior and phase transformation during the precipitation of calcium carbonate minerals from intermediate ionic solutions at 25 °C. *Geochim. Cosmochim. Acta* **65**, 3219–3231.

Johnson K., Hu C., Belshaw N. and Henderson G. (2006) Seasonal trace-element and stable-isotope variations in a Chinese speleothem: the potential for high-resolution paleomonsoon reconstruction. *Earth Planet. Sci. Lett.* **244**, 394–407.

Keeling C. (1958) The concentration and isotopic abundances of atmospheric carbon dioxide in rural areas. *Geochim. Cosmochim. Acta* **13**, 322–334.

Kim S. T. and O'Neil J. R. (1997) Equilibrium and nonequilibrium oxygen isotope effects in synthetic carbonates. *Geochim. Cosmochim. Acta* **61**, 3461–3475.

Kim S. T., Hillaire-Marcel C. and Mucci A. (2006) Mechanisms of equilibrium and kinetic oxygen isotope effects in synthetic aragonite at 25 °C. *Geochim. Cosmochim. Acta* **70**, 5790–5801.

Kim S. T., Mucci A. and Taylor B. (2007) Phosphoric acid fractionation factors for calcite and aragonite between 25 and 75 °C: revisited. *Chem. Geol.* **246**, 135–146.

Kowalczk A. (2009) High resolution microclimate study of hollow ridge cave: relationships between cave meteorology, air chemistry, and hydrology and the impact on speleothem deposition. Master's thesis, Florida State University, Department of Oceanography. Available from: <http://etd.lib.fsu.edu/theses/available/etd-10212009-010946/>.

Kowalczk A. and Froelich P. (2010) Cave air ventilation and CO_2 outgassing by radon-222 modeling: how fast do caves breathe? *Earth Planet. Sci. Lett.* **289**, 209–219.

Lachniet M. S., Burns S. J., Pipemo D. R., Asmerom Y., Polyak V. J., Moy C. M. and Christenson K. (2004a) A 1500-year El Nino/Southern Oscillation and rainfall history for the Isthmus of Panama from speleothem calcite. *J. Geophys. Res.* **109**. doi:10.1029/2004JD004694.

Lachniet M. S., Asmerom Y., Burns S. J., Patterson W. P., Polyak V. J. and Seltzer G. O. (2004b) Tropical response to the 8200 yr B.P. cold event? Speleothem isotopes indicate a weakened early Holocene monsoon in Costa Rica. *Geology* **32**, 957–960.

Lachniet M. S. (2009) Climatic and environmental controls on speleothem oxygen-isotope values. *Quatern. Sci. Rev.* **28**, 412–432.

Lambert W. J. (2010) High resolution, U/Th dated (32,000 to 11,000 years), oxygen and carbon isotope proxy climate records from a stalagmite in DeSoto Caverns, Alabama, USA. Ph. D. dissertation, University of Alabama, 249 pp.

Lambert W. J. and Aharon P. (2010) Oxygen and hydrogen isotopes of rainfall and dripwater at DeSoto Caverns (Alabama, USA): key to understanding past variability of moisture transport from the Gulf of Mexico. *Geochim. Cosmochim. Acta* **74**, 846–861.

Lambert W. and Aharon P. (2011) Controls on dissolved inorganic carbon and $\delta^{13}C$ in cave waters from DeSoto Caverns: implications for speleothem $\delta^{13}C$ assessments. *Geochim. Cosmochim. Acta* **75**, 753–768.

Maddox G. (1993) *Karst features of Florida Caverns State Park and Falling Waters State Recreation Area; Jackson and Washington counties, Florida*. Southeastern Geological Survey, Tallahassee, FL, pp. 38.

Mangini A., Spötl C. and Verdes P. (2005) Reconstruction of temperature in the Central Alps during the past 2000 yr from a $\delta^{18}O$ stalagmite record. *Earth Planet. Sci. Lett.* **235**, 741–751.

Mangini A., Blumbach P., Verdex P., Spötl C., Scholz D., Machel H. and Mahon S. (2007) Combined records from a stalagmite from Barbados and from Lake sediments in Haiti reveal variable seasonality in the Caribbean between 6.7 and 3 ka BP. *Quatern. Sci. Rev.* **26**, 1332–1343.

Mattey D., Lowry D., Duffet J., Fisher R., Hodge E. and Frisia S. (2008) A 53 year seasonally resolved oxygen and carbon isotope record from a modern Gibraltar speleothem: reconstructed drip water and relationship to local precipitations. *Earth Plant. Sci. Lett.* **269**, 80–95.

Matthews A., Ayalon A. and Bar-Matthews M. (2000) D/H ratios of fluid inclusions of Soreq cave Israel speleothems as a guide to the Eastern Mediterranean Meteoric Line relationships in the last 120 ky. *Chem. Geol.* **166**, 183–191.

McCrea J. M. (1950) On the isotopic chemistry of carbonates and a paleotemperature scale. *J. Chem. Phys.* **18**, 849–858.

McDermott F. (2004) Palaeo-climate reconstruction from stable isotope variations in speleothems: a review. *Quatern. Sci. Rev.* **23**, 901–918.

McDermott F., Schwarcz H. P., Harmon R. S., Thompson P. and Ford D. C. (2006) Isotopes in speleothems. In *Isotopes in Paleoenvironmental Research. Developments in Paleoenvironmental Research* (ed. M. J. Leng). Springer, Dordrecht, The Netherlands, pp. 185–225.

McGarry S., Bar-Matthews M., Matthews A., Vaks A., Schilman B. and Ayalon A. (2004) Constraints on hydrological and paleotemperature variations in the Eastern Mediterranean region in the last 140 ka given by the δD values of speleothem fluid inclusions. *Quatern. Sci. Rev.* **23**, 919–934.

Mickler P. J., Banner J. L., Stern L., Asmerom Y., Edwards R. L. and Ito E. (2004) Stable isotope variations in modern tropical speleothems: evaluating equilibrium vs. kinetic isotope effects. *Geochim. Cosmochim. Acta* **68**, 4381–4393.

Mickler P. J., Stern L. A. and Banner J. L. (2006) Large kinetic isotope effects in modern speleothems. *GSA Bull.* **118**, 65–81.

Mook W. and de Vriess J. (2000). Introduction. Theory, methods, review. In *Environmental Isotopes in the Hydrological Cycle. Principles and Applications* **vol. 1**, IAEA.

Mühlinghaus C., Scholz D. and Mangini A. (2009) Modelling fractionation of stable isotopes in stalagmites. *Geochim. Cosmochim. Acta* **73**, 7275–7289.

Musgrove M. and Banner J. (2004) Controls on the spatial and temporal variability of vadose dripwater geochemistry: Edwards Aquifer, central Texas. *Geochim. Cosmochim. Acta* **68**, 1007–1020.

O'Neil J. R., Clayton R. N. and Mayeda T. K. (1969) Oxygen isotope fractionation in divalent metal carbonates. *J. Chem. Phys.* **51**, 5547–5558.

O'Neil J. R. and Truesdell A. H. (1991) Oxygen isotope fractionation studies of solute–water interactions. *Geochem. Soc. Spec. Pub.* **3**, 17–25.

Oster J., Montanez I., Guilderson T., Sharp W. and Banner J. (2010) Modeling speleothem $\delta^{13}C$ variability in a central Sierra Nevada cave using ^{14}C and $^{87}Sr/^{86}Sr$. *Geochim. Cosmochim. Acta* **74**, 5228–5242.

Pape J., Banner J., Mack L., Musgrove M. and Guilfoyle A. (2010) Controls on oxygen isotope variability in precipitation and cave drip waters, central Texas, USA. *J. Hydrol.* **385**, 203–215.

Partin J. W., Cobb K. M., Adkins J. F., Clark B. and Fernandez D. P. (2007) Millennial-scale trends in west Pacific warm pool hydrology since the Last Glacial Maximum. *Nature* **449**, 452–455.

Patterson W. P., Smith G. R. and Lohmann K. C. (1993) Continental Paleothermometry and seasonality using the isotopic composition of aragonitic otoliths of freshwater fishes. In *Climate Change in Continental Isotopic Records* (eds. P. K. Swart et al.). Geophys. Monogr. Ser. **78**, pp. 191–202.

Paul D. and Skrzypek G. (2007) Assessment of carbonate-phosphoric acid analytical technique performed using GasBench II in continuous flow isotope ratio mass spectrometry. *Int. J. Mass. Spec.* **262**, 180–186.

Perrier F., Richon P. and Sabroux J. (2005) Modelling the effect of air exchange on ^{222}Rn and its progeny concentration in a tunnel atmosphere. *Sci. Total Environ.* **350**, 136–150.

Pflitsch A. and Piasecki J. (2003) Detection of an airflow system in Niedzwiedzia (Bear) Cave, Kletno, Poland. *J. Cave Karst Stud.* **65**, 160–173.

Pilson M. Q. (1998) *An Introduction to the Chemistry of the Sea*, first ed. Prentice Hall.

Plagnes V., Causse C., Genty D., Paterne M. and Blamart D. (2002) A discontinuous climatic record from 187 to 74 ka from a speleothem of the Clamouse Cave (South of France). *Earth Planet. Sci. Lett.* **201**, 87–103.

Plummer L., Busenburg E. and Riggs A. (2000) In-situ growth of calcite at Devils Hole, Nevada: comparison of field and laboratory rates to a 500,000 year record of near-equilibrium calcite growth. *Aqua. Geochem.* **6**, 257–274.

Polag D., Scholz D., Mühlinghaus C., Spötl C., Schroder-Ritzrau A., Segl M. and Mangini A. (2010) Stable isotope fractionation in speleothems: laboratory experiments. *Chem. Geol.* **279**, 31–39.

Poore R., Dowsett H., Verardo S. and Quinn T. (2003) Millennial- to century-scale variability in the Gulf of Mexico Holocene climate records. *Paleoceanography* **18**, 26-1–26-13.

Poore R., Quinn T. and Verardo S. (2004) Century-scale movement of the Atlantic Intertropical Convergence Zone linked to solar variability. *Geophys. Res. Lett.* **31**, L12211–L12214.

Poore R. Z., DeLong K. L., Richey J. N. and Quinn T. M. (2009) Evidence of multidecadal climate variability and the Atlantic Multidecadal Oscillation from a Gulf of Mexico sea-surface temperature-proxy record. *Geo-Mar. Lett.* **29**, 477–484.

Poulson T. L. and White W. B. (1969) The cave environment. *Science* **165**, 971–981.

Richey J., Poore R., Flower B. and Quinn T. (2007) 1400 yr multiproxy record of climate variability from the northern Gulf of Mexico. *Geology* **35**, 423–436.

Richey J. N., Poore Richard Z., Flower B. P., Quinn T. M. and Hollander D. J. (2009) Regionally coherent Little Ice Age cooling in the Atlantic Warm Pool. *Geophys. Res. Lett.* **36**, 21701–21705.

Richon P., Perrier F., Sabroux J., Trique M., Ferry C., Voisin V. and Pili E. (2005) Spatial and time variations of radon-222 concentration in the atmosphere of a dead-end horizontal tunnel. *J. Environ. Radioactiv.* **78**, 179–198.

Rowe P. J., Dennis P. F., Atkinson T. C., Lauritzen S. E. and Lundberg J. (1998) A high resolution deuterium record from fluid inclusions in a late Holocene speleothem from S.W. Britain. In *Proceedings, PAGES Open Science Meeting*. University of London. 112 p.

Scholz D., Mühlinghaus C. and Mangini A. (2009) Modelling $\delta^{13}C$ and $\delta^{18}O$ in the solution layer on stalagmite surfaces. *Geochim. Cosmochim. Acta* **73**, 2592–2602.

Schulz K., Riebesell U., Rost B., Thoms S. and Zeebe R. (2006) Determination of the rate constants for the carbon dioxide to bicarbonate inter-conversion in pH-buffered seawater systems. *Mar. Chem.* **100**, 53–65.

Schwarcz H. P., Harmon R. S., Thompson P. and Ford D. C. (1976) Stable isotope studies of fluid inclusions in speleothems and their paleoclimatic significance. *Geochim. Cosmochim. Acta* **40**, 657–665.

Schwarcz H. P. (1986) Geochronology and isotopic geochemistry of speleothems. *Handbook Environ. Isotope Geochem.* **2**, 271–303 (Chapter 7).

Sharp Z. (2007) *Principles of Stable Isotope Geochemistry*. Pearson Education Inc., pp. 344.

Sinha A., Cannariato K. G., Stott Lowell. D., Cheng H., Edwards R. L., Yadava M. G., Ramesh R. and Singh I. B. (2007) A 900-year (600 to 1500 A.D.) record of the Indian summer monsoon precipitation from the core monsoon zone of India. *Geophys. Res. Lett.* **34**, L16707.

Spötl C., Fairchild I. J. and Tooth A. (2005) Cave air control on dripwater geochemistry, Obir Caves (Austria): implications for speleothem deposition in dynamically ventilated caves. *Geochim. Cosmochim. Acta* **69**, 2451–2468.

Tarutani T., Clayton R. N. and Mayeda T. K. (1969) The effect of polymorphism and magnesium substitution on oxygen isotope fractionation between calcium carbonate and water. *Geochim. Cosmochim. Acta* **33**, 987–996.

Teng H., Dove P. and De Yoreo J. (2000) Kinetics of calcite growth: surface processes and relationships to macroscopic rate laws. *Geochim. Cosmochim. Acta* **64**, 2255–2266.

Treble P., Shelley J. M. G. and Chappell J. (2003) Comparison of high resolution sub-annual records of trace elements in a modern (1911–1992) speleothem with instrumental climate data from southwest Australia. *Earth Planet. Sci. Lett.* **216**, 141–153.

Tremaine D. M. (2010) Speleothem paleoclimatology and modern speleochemistry proxies: calcite farming in a continuously monitored cave. Master's thesis, Florida State University, Department of Oceanography. Available from: <http://etd.lib.fsu.edu/theses/available/etd-07052010-230757/>.

Urey H. C. (1947) The thermodynamic properties of isotopic substances. *J. Chem. Soc.* **1**, 562–581.

Urey H. C. (1948) Oxygen isotopes in nature and in the laboratory. *Science* **108**, 489–496.

van Beynen P., Asmerom Y., Polyak V., Soto L. and Polk J. (2007) Variable intensity of teleconnections during the late Holocene in subtropical North America from an isotopic study of speleothems from Florida. *Geophys. Res. Lett.* **34**, L18703.

van Beynen P. E., Soto L. and Pace-Graczyk K. (2008) Paleoclimate reconstruction derived from speleothem strontium and $\delta^{13}C$ in Central Florida. *Quatern. Int.* **187**, 76–83.

van Breukelen M. R., Vonhof H. B., Hellstrom J. C., Wester W. C. G. and Kroon D. (2008) Fossil dripwater in stalagmites reveals Holocene temperature and rainfall variation in Amazonia. *Earth Planet. Sci. Lett.* **275**, 54–60.

Vonhof H. B., van Breukelen M. R., Postma O., Rowe P. J., Atkinson T. C. and Kroon D. (2006) A continuous-flow crushing device for on-line δ^2H analysis of fluid inclusion water in speleothems. *Rapid Commun. Mass Spectrom.* **20**, 2553–2558.

Wang X., Auler A. S., Edwards R. L., Cheng H., Cristalli P. S., Smart P. L., Richards D. A. and Shen C. (2004) Wet periods in northeastern Brazil over the past 210 kyr linked to distant climate anomalies. *Nature* **432**, 740–743.

Wang Y., Cheng H., Edwards R. L., He Y., Kong X., An Z., Wu J., Kelly M. J., Dykoski C. A. and Li X. (2005) The holocene Asian monsoon: links to solar changes and North Atlantic climate. *Science* **308**, 854–857.

Wang Y., Cheng H., Edwards R. L., Kong X., Shao X., Chen S., Wu J., Jiang X., Wang X. and An Z. (2008) Millennial and orbital-scale changes in the East Asian monsoon over the past 224,000 years. *Nature* **451**, 1090–1093.

Wang Y. J., Cheng H., Edwards R. L., An Z. S., Wu J. Y., Shen C. C. and Dorale J. A. (2001) A high-resolution absolute-dated late pleistocene monsoon record from Hulu Cave, China. *Science* **294**, 2345–2348.

Watson E. B. (2004) A conceptual model for near-surface kinetic controls on the trace-element and stable isotope composition of abiogenic calcite crystals. *Geochim. Cosmochim. Acta* **68**, 1473–1488.

Watts W. and Hansen B. (1994) Pre-holocene and holocene pollen records of vegetation history from the Florida peninsula and their climatic implications. *Paleogeogr. Paleoclimatol. Paleoecol.* **109**, 163–176.

Werner R. and Brand W. (2001) Referencing strategies and techniques in stable isotope ratio analysis. *Rapid Commun. Mass Spectrom.* **15**, 501–519.

Wiedner E., Scholz D., Mangini A., Polag D., Mühlinghaus C. and Segl M. (2008) Investigation of the stable isotope fractionation in speleothems with laboratory experiments. *Quatern. Int.* **187**, 15–24.

Willard D., Bernhardt C., Brooks G., Cronin T., Edgar T. and Larson R. (2007) Deglacial climate variability in central Florida, USA. *Paleogeogr. Paleoclimatol. Paleoecol.* **251**, 366–382.

Winograd I. J., Coplen T. B., Landwehr J. M., Riggs A. C., Ludwig K. R., Szabo B. J., Kolesar P. T. and Revesz K. M. (1992) Continuous 500,000-year climate record from vein calcite in Devils Hole, Nevada. *Science* **258**, 255–260.

Wong C., Banner J. and Musgrove M. (2011) Seasonal dripwater Mg/Ca and Sr/Ca variations driven by cave ventilation: implications for and modeling of speleothem paleoclimate records. *Geochim. Cosmochim. Acta.* **75**, 3514–3529.

Yu J., Day J., Greaves M. and Elderfield H. (2005) Determination of multiple element/calcium ratios in formainiferal calcite by quadrupole ICP-MS. *G*^{3} **6**, pp 9.

Zeebe R., Wolf-Gladrow D. and Jansen H. (1999) On the time required to establish chemical and isotopic equilibrium in the carbon dioxide system in seawater. *Mar. Chem.* **65**, 135–153.

Zhang R., Schwarcz H. P., Ford D. C., Schroeder F. S. and Beddows P. A. (2008) An absolute paleotemperature record from 10 to 6 Ka inferred from fluid inclusion D/H ratios of a stalagmite from Vancouver Island, British Columbia, Canada. *Geochim. Cosmochim. Acta* **72**, 1014–1026.

Ziegler M., Nurnberg D., Karas C., Tiedemann R. and Lourens L. (2008) Persistent summer expansion of the Atlantic Warm Pool during glacial abrupt cold events. *Nat. Geosci.* **1**, 601–605.

Associate editor: Miryam Bar-Matthews